CONTRACTOR REPORT

SAND82-7003/1
Unlimited Release
UC-66c

Advanced Wellbore Thermal Simulator GEOTEMP2 Research Report

SAND--82-7003/1

DE82 020050

Robert F. Mitchell
Enertech Engineering and Research Co.
Houston, TX 77098

Prepared by Sandia National Laboratories Albuquerque, New Mexico 87185 and Livermore, California 94550 for the United States Department of Energy under Contract DE-AC04-76DP00789

Printed February 1982

Issued by Sandia National Laboratories, operated for the United States Department of Energy by Sandia Corporation.

Printed in the United States of America
Available from
National Technical Information Service
U.S. Department of Commerce
5285 Port Royal Road
Springfield, VA 22161

NTIS price codes
Printed copy: A02
Microfiche copy: A01

DISCLAIMER

ADVANCED WELLBORE THERMAL SIMULATOR

GEOTEMP2

RESEARCH REPORT

By

Robert F. Mitchell

Enertech Engineering and Research Co.

Houston, Texas

Sandia Laboratories Contract 46-5670

Department of Energy

Geothermal Technology Development

Division 4741

ADVANCED WELLBORE THERMAL SIMULATOR

GEOTEMP2

RESEARCH REPORT

Robert F. Mitchell

Sandia Laboratories Contract 46-5670

December 1981

ABSTRACT

This report describes the development of the GEOTEMP2 wellbore thermal simulator. The major technical features include a general purpose air and mist drilling simulator and a two-phase steam flow simulator that can model either injection or production.

An improved method for calculating downhole temperatures, pressures, fluid densities and velocities during air drilling has been developed. Improvements on previous methods include:

1. A fully transient thermal analysis of the wellbore and formation is used to determine the flowing temperatures.

2. The effects of flow acceleration are included explicitly in the calculation.

3. The slip velocity between the gas and the cuttings is determined by the use of a separate momentum equation for the cuttings.

4. The possibility of critical flow in the wellbore is tested for and appropriate changes in the volume flow rate and standpipe pressure are made automatically

5. The standpipe and flowing pressures are predicted.

6. The analysis is conservative. The effect of the cuttings on the wellbore flow will tend to overpredict the required volume flow rates.

In this report, the basic equations of fluid flow for a gas with cuttings and mist are presented along with a numerical method for their solution. Several applications of this calculational method are given, showing the effect of flow rate and standpipe pressure in typical air and mist drilling situations.

The philosophy used in the development of the steam injection/production model was not to work from first principles, as in the gas drilling model, but rather to program the best available flow correlations. Two-phase flow is sufficiently complicated that there are few analytic solutions to even very restricted flow types. As a result, correlations of experimental data have been the usual method

for the analysis of two-phase flow.

The section on two-phase flow details one of the better sets of flow correlations with claimed accuracy of less than 10% error. Equally important to the steam flow model are the thermodynamic and transport property correlations. These correlations are the same ones used to generate steam tables and are very accurate.

TABLE OF CONTENTS

ACKNOWLEDGEMENTS

I would like to thank Al Ortega of Sandia Laboratories for suggestions and management during this work. I would also like to thank Lisa Mondy of Sandia Laboratories for her help with the program debugging. The work reported here was funded by Sandia Laboratories.

NOMENCLATURE

A = flow cross-sectional area

a, b, c = coefficients in flow equation

C_D = cuttings drag coefficient

d = average cutting diameter

D = hydraulic diameter of the duct

f = D'Arcy friction factor

F = frictional pressure drop

g = gravity constant

G = mass flux density of air

G_g = mass flux density of vapor

G_s = mass flux density of cuttings

G_w = mass flux density of liquid water

K = thermal conductivity

$(L)_B$ = the bubble flow/slug flow boundary number

$(L)_M$ = the transition flow/mist flow boundary number

$(L)_S$ = the slug flow/transition flow boundary number

$\dot{m}$ = mass flow rate of air

$\dot{m}_s$ = mass flow rate of cuttings

N_{Nu} = Nusselt number

N_{Pr} = Prandtl number

N_{Re} = Reynolds number

P = air force on cuttings

P_0, P_1 = coefficients in P equation

Q = heat flux per unit length

R = ideal gas constant

T = absolute temperature

V = velocity of air

v_b = bubble rise velocity

$\tilde{v}_g$ = the dimensionless gas velocity

V_{ns} = the no-slip velocity

V_s = velocity of cuttings

V_{Sg} = the superficial gas velocity

V_{Sw} = the superficial liquid velocity

v_w = bubble flow actual liquid velocity

W = gravitational pressure drop

W_s = cuttings gravity pressure drop

W_0 = coefficient in W_s equation

Z = coordinate along duct axis

δ = ratio of particle volume to particle cross-sectional area

γ = slug flow liquid distribution coefficient

ρ = air density

ρ_g = water vapor density

ρ_w = liquid water density

ρ_s = cutting particle density

$\bar{\rho}$ = in-mixture air density

$\bar{\rho}_s$ = in-mixture cuttings density

ϕ = volume fraction of cuttings

ϕ_g = volume fraction vapor

σ = water/steam surface tension

θ = duct inclination from vertical

ω = two-phase average flowing density

τ_f = two-phase frictional gradient

Subscript nomenclature:

b bubble

g water vapor

s cuttings

tp two-phase

w liquid water

1 inlet conditions

2 exit conditions

e.g. V_{s_2} is the exit cuttings velocity,

V_1 is the inlet air velocity.

LIST OF FIGURES

INTRODUCTION

This report discusses the technical features of the wellbore thermal simulator GEOTEMP2. GEOTEMP2 was developed from GEOTEMP under Sandia Laboratories contract 46-5670. The original GEOTEMP was also developed for Sandia under contract 13-0212 and reported in reference [9]. GEOTEMP represents a fairly basic wellbore thermal simulator. The temperatures predicted are fully transient in the wellbore and the formation, but the fluids circulating in the wellbore are restricted to incompressible liquids. Geothermal applications have needs beyond this basic simulation ability. In particular, drilling with compressible fluids such as air or nitrogen is common. The production of steam, a multi-phase compressible fluid, is the principal goal of geothermal development. The flow models discussed here were developed by Enertech Engineering and Research Co. for use in this general purpose wellbore thermal simulator called GEOTEMP2. Some features of GEOTEMP, an earlier version of GEOTEMP2, have have been described in previous papers (references [2] and [3]). The major technical features in the new version, GEOTEMP2, are summarized in the following:

1. The flowing stream energy balance is fully transient, that is, temperature predictions are accurate for short time intervals. The thermal analysis is not 'steady state'.

2. The thermal properties of the wellbore are fully described, including the steel, cement, and fluids in real well

completions. The program is sufficiently general to describe most wells.

3. The temperature calculations in the wellbore and the surrounding formation are directly coupled.

4. The code has been designed with enough flexibility so that the complete life of a well from drilling to production, shut-ins for workovers, injection, etc. can be simulated in one computer run.

5. Several different wellbore fluids can be specified, such as drilling muds, packer fluids, cements, and production fluids. Further, more than one fluid may be in the wellbore at the same time, and the displacement of one fluid by another is automatically determined. The simulation of cement operations is one possible application.

6. Two-phase steam production and injection can be simulated with GEOTEMP2. Flowing stream properties and flow types (e.g. slug flow) are determined as well as flow temperatures.

7. Air, nitrogen, and mist drilling can be simulated. This analysis is described in this paper. GEOTEMP2 can switch between air and mud drilling at any time desired.

The GEOTEMP2 thermal simulator has been thoroughly tested against

analytic solutions and field data.

Air and Mist Drilling

Air and mist drilling have several advantages over conventional drilling fluids for geothermal drilling. The principle advantages are higher penetration rates, longer bit life, and no lost circulation problems. The usual disadvantages, such as control of fluid influx and high pressure zones, are not normally a factor in geothermal well drilling.

To realize these advantages, it is important to maintain adequate circulation. Determining the required volume flow rate to maintain this 'adequate' circulation has always been difficult. The best available technique has been the chart developed by R. R. Angel [1]. This chart allows the estimation of volume circulation rates for various hole sizes, drill pipe sizes, and penetration rates.

One difficulty with Angel's result is that the equation giving the volume flow rate must be solved by trial and error. This difficulty is avoided by using the charts prepared by Angel, provided the case of interest is tabulated or can be estimated from similar cases. A second difficulty is that the drill cuttings are assumed to travel at the same velocity as the air. Angel notes that this is not a conservative assumption and the analysis presented here demonstrates that the flow rates he predicts are 20 to 30 percent low. The downhole temperatures used for Angel's chart are assumed to be 80 degrees F at the surface,

increasing 1 degree F per 100 feet of depth. There is no convenient way to convert to other temperatures. A final consideration is that the Angel charts do not apply to mist drilling. The addition of water to the air requires increases in both the volume flow rate and standpipe pressures to maintain the same penetration rate.

In this report, the equations of compressible gas flow are solved by an integral equation method. This method is discussed in the section of this report titled Compressible Flow. In this section, the flow equations are solved and compared to known analytic solutions. In the next section, Gas Drilling, the appropriate modifications necessary to incorporate drill cuttings and mist in the air drilling model are discussed. The model results are compared to Angel's analysis and a sample problem is used to demonstrate applications to geothermal drilling.

Two-Phase Steam Injection/Production

The last section of this report describes the two-phase flow models used to simulate the production and injection of steam. This analysis requires three basic parts. First, a complete set of thermodynamic and transport property correlations are needed. Steam and water represent difficult materials to describe analytically, so simple property correlations, as used in the gas drilling models, are not adequate. The correlations used in GEOTEMP2 are based on the equations used to produce Steam Tables by Keenan, Keyes, et.al. (reference [14]). These are the best, most accurate correlations

available that can also be computed efficiently. The correlations used in GEOTEMP2 are fully described in Appendix D.

The second basic part of the steam models is the vertical pressure drop correlations. The flowing presssure of a two-phase steam mixture determines the temperature, and thus all of the heat transfer properties. The determination of the flowing pressure is not simple, for example, there are four recognized types of flow for two-phase mixtures. The philosophy taken for work in this section was to program the best available correlation rather than work from first principles, as in the gas drilling section. One of the best vertical flow two-phase pressure drop correlations was developed by Orkiszewski, (reference [10]). This correlation is discussed in depth in the section Two-Phase Flow of Steam.

The last part of the two-phase steam model is the heat transfer correlation. The Case I method developed by Duckler (reference [13]) was chosen because it was consistent with the single phase flow correlation used by GEOTEMP2 , consistent with theoretical analysis of two-phase flow, and relatively simple to implement.

COMPRESSIBLE FLOW MODEL

The subsonic flow of a compressible fluid can often produce results that seem to go counter to common sense. For instance, consider the steady flow of air in a constant area duct.As with all fluids, there is a pressure loss due to friction, and the pressure decreases continuously from the entrance of the duct to the exit. Unlike the flow of incompressible fluids, the fluid velocity increases from the entrance of the duct to the exit.

Two facts account for this acceleration. First, the gas pressure is proportional to the density (as in the ideal gas law $P=\rho RT$). As the pressure of the gas decreases, the density must decrease also. Second, since the mass flow through the duct is constant, the product of density and velocity is constant . Thus, as the density decreases with the pressure, the velocity must increase to maintain the mass flow. (In supersonic flow, the dynamic pressure term reverses this effect)

This example demonstrates a typical compressible flow characteristic, the interrelationship of pressure and mass flow. In air drilling, high velocities are needed at bottom hole to remove the cuttings. High velocities result in friction pressure drops in the drill pipe and annulus, so higher standpipe pressures may be needed to

keep the air flowing. It would be very useful to be able to evaluate these effects to better plan an air drilling operation.

The flow of a compressible fluid is described by the three conservation laws of fluid mechanics: the balance of mass, momentum, and energy. For simplicity, this discussion will only consider the balance of mass and momentum, similar to Angel's analysis for steady flow. For a complete discussion of the balance laws, reference [4] provides the general equations and many useful special applications.

Figure 1 illustrates the flow of a compressible fluid in a constant area duct. The duct has cross-sectional area A and length ΔZ. The fluid entering this section of duct has flow properties denoted by the subscript 1, while the exit properties have the subscript 2. The gravity force is directed against the flow and the duct is inclined to the gravity force by the angle θ.

The balance of mass for steady flow has the form:

$$\rho V A = \dot{m} = \text{constant} \tag{1}$$

which says that the mass flow rate $\dot{m}$ is constant. The symbol G is used to denote a convenient quantity called the mass flux density:

$$G = \rho V, \tag{2}$$

and G is constant for constant area ducts by equation (1).

The balance of momentum can be expressed in the following form:

$$P_2 - P_1 + G[V_2 - V_1] + F + W = 0 \qquad (3)$$

where

$$F = \frac{1}{2}\frac{f}{D}\int_{z_1}^{z_2} GV\,dZ \qquad (4)$$

and

$$W = \int_{z_1}^{z_2} \rho g \cos\theta \; dZ \qquad (5)$$

The term F in equation (3) is the pressure drop due to frictional losses and term W is the pressure drop due to gravity loads. D is the hydraulic diameter, which is equal to the inside diameter for tubing and equal to the difference between the outside and inside diameters for the annulus. The term f is the D'Arcy friction factor. This factor can be evaluated from friction factor charts called Moody diagrams (see reference 4, pages 256-257) or by use of analytic expressions (see Appendix A).

An additional relationship needed to solve equation (3) is an equation of state for the gas. For air drilling applications, air is very nearly an ideal gas, so

$$P = \rho RT \qquad (6)$$

is the neeeded equation. Equation (2) can be used to eliminate density from equations (3) and (5). The temperature of the flowing fluid is assumed to be known in this discussion. Angel assumed that the temperature of the fluid was equal to the undisturbed geothermal temperature. In general, the energy equation needs to be solved simultaneously with the mass and momentum equations to obtain the temperature. If the temperature is known, equation (3) is now reduced to a non-linear integral equation for the velocity. When the velocity has been determined, the remaining flow variables can be determined through equations (2) and (6).

The method of weighted residuals is used to solve equation (3) for the exit velocity. A weighting function equal to the constant 1 was used. To apply the method, the total duct length is subdivided into cells. Across each cell, the velocity is assumed to vary linearly:

$$V(Z) = V_1 + (V_2 - V_1)(Z - Z_1)/(Z_2 - Z_1) \qquad (7)$$

Equations (4) and (5) can now be evaluated in terms of the inlet flow properties and the unknown exit velocity V_2. Equation (5) integrates to the logarithm of the ratio of V_2 to V_1, however, this can be approximated by:

$$W = \rho_1 \cos\theta \left[\frac{3}{2} - \frac{1}{2}\frac{V}{V_1}^2 \right] \Delta Z \qquad (8)$$

with an error of the order of $(V_1-V_2)/V_1$ cubed.

The resulting equation for V_2 is the following quadratic:

$$a(V_2)^2 + bV_2 + c = 0 \tag{9}$$

where:

$$a = G - \frac{1}{2V_1}\left[\rho_1 g\cos\theta + \frac{1G}{2D}fV_1\right]\Delta Z \tag{10}$$

$$b = -P_1-GV_1+ \frac{1}{2}\left[3\rho_1 g\cos\theta + \frac{1G}{2D}fV_1\right]\Delta Z \tag{11}$$

$$c = GRT_2 \tag{12}$$

Equation (9) can be solved easily for the exit velocity V_2:

$$V_2 = -(b+(b^2-4ac)^{\frac{1}{2}})/2a \tag{13}$$

Equation (13) does not have a real solution for negative values of the determinant b^2-4ac. The physical sense of a negative determinant is that the flow has 'choked', that is, there is not enough pressure to support the assumed mass flow rate. Either the inlet pressure needs to be increased or the flow rate decreased until the determinant is positive.

This numerical model was tested against analytic solutions of the compressible flow equations. There are three ways of obtaining closed form solutions of the compressible flow equations. The first method is to neglect heat transfer in the energy equation, which can then be directly integrated. The momentum equation can then be reduced to an

equation in a single variable and solved. The second method is to neglect the frictional pressure drop term in the momentum equation. The energy equation can now be reduced to a single variable and solved. The third method is to define the temperature to be constant and solve the momentum equation. (A fourth method would be to define the density to be constant, but the physical signifigance of this solution would be even less than the other three.) It is clear that these methods do not provide a way to include all dissipative effects in one closed form solution.

The model comparisons all have the following basic data in common:

Inlet pressure: 700 KPa

Inlet temperature: 26.85 C

Inlet velocity: 15 M/S

Duct length: 5000 M

These conditions were chosen to be characteristic of air drilling operations. Two numerical solutions were prepared for each test case: two 2500 M elements for one case and five 1000 M elements for a second comparison case. The first case demonstrates the performance of the numerical model for a relatively coarse subdivision. The second case is intended to show convergence to the analytic solution with increased number of subdivisions.

Figures 2,3, and 4 compare the velocity, pressure, and temperature predictions of the numerical model to the adiabatic flow with friction

solution. The numerical model underpredicts the velocity changes by about 1% for the coarse subdivision and improves to 1/2% for the finer subdivision. This response is typical of this type of numerical solution and is usually attributed to the reduced number of degrees of freedom compared to the full continuum solution. As a direct result of underpredicting the velocity changes, the pressure drop in the duct is also underpredicted. Figure 3 shows the duct pressures predicted by the numerical model to be about 1% high for the coarse subdivision, converging to the analytical solution for finer subdivisions. Figure 4 shows the temperature changes to be underpredicted, consistent with the results for the velocities and pressures. As in the other cases, the error for even the coarsest subdivision is very low.

Figures 5,6,and 7 compare the velocity, pressure, and temperature predictions of the numerical model to the analytic solution for frictionless flow with heat transfer. It should not be surprising that the numerical model matches the analytic solution almost perfectly, since the frictional pressure drop term has been deleted. The very slight error in the pressure predictions is due to numerical round off. The mathematical expression of the analytic solution is equivalent to the numerical solution in this case, but the closed form solution had to be solved numerically, resulting in small round off errors.

Figures 8 and 9 compare the velocity and pressure predictions of the numerical model to the analytical solution for isothermal flow with friction. The results are comparable with the adiabatic flow solution because the energy equation in that case has been replaced by defining

the temperature to be constant. The momentum equation remains unchanged. The model predictions for the velocities and pressures are of the same accuracy as the adiabatic model results. Generally, the model results were very accurate, even for relatively coarse subdivisions. The model underpredicted velocity changes but converged to the analytic solution for finer subdivisions of the duct length.

Figure 1. Constant Area Flow Cell

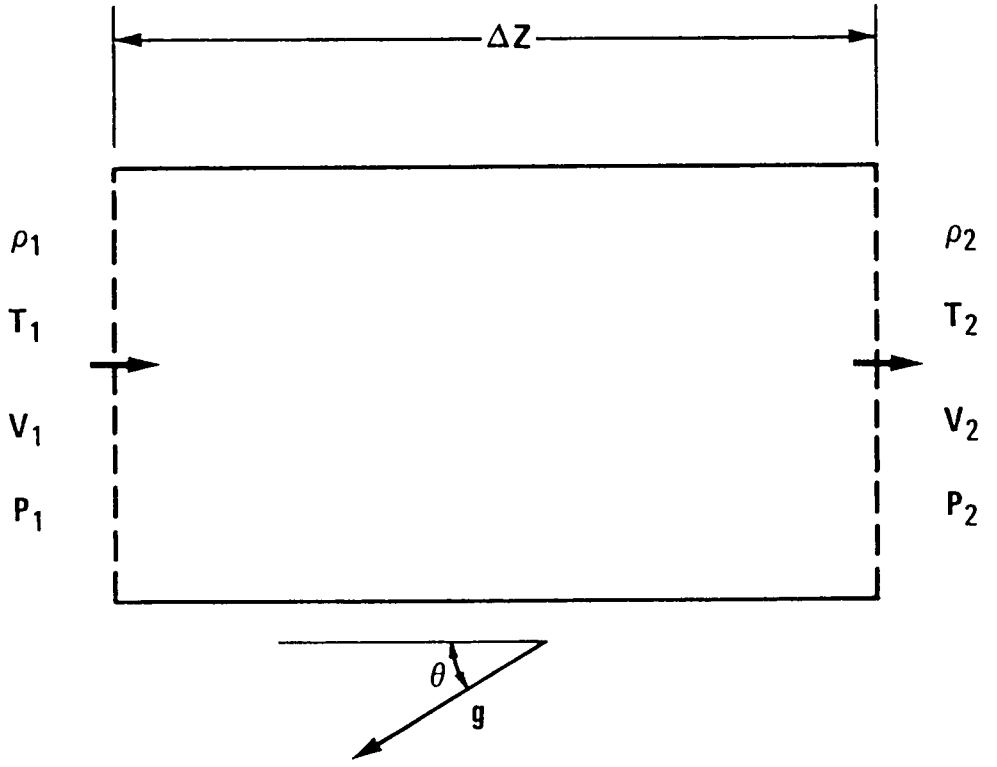

Figure 2. Flow Velocities: Adiabatic Flow with Friction

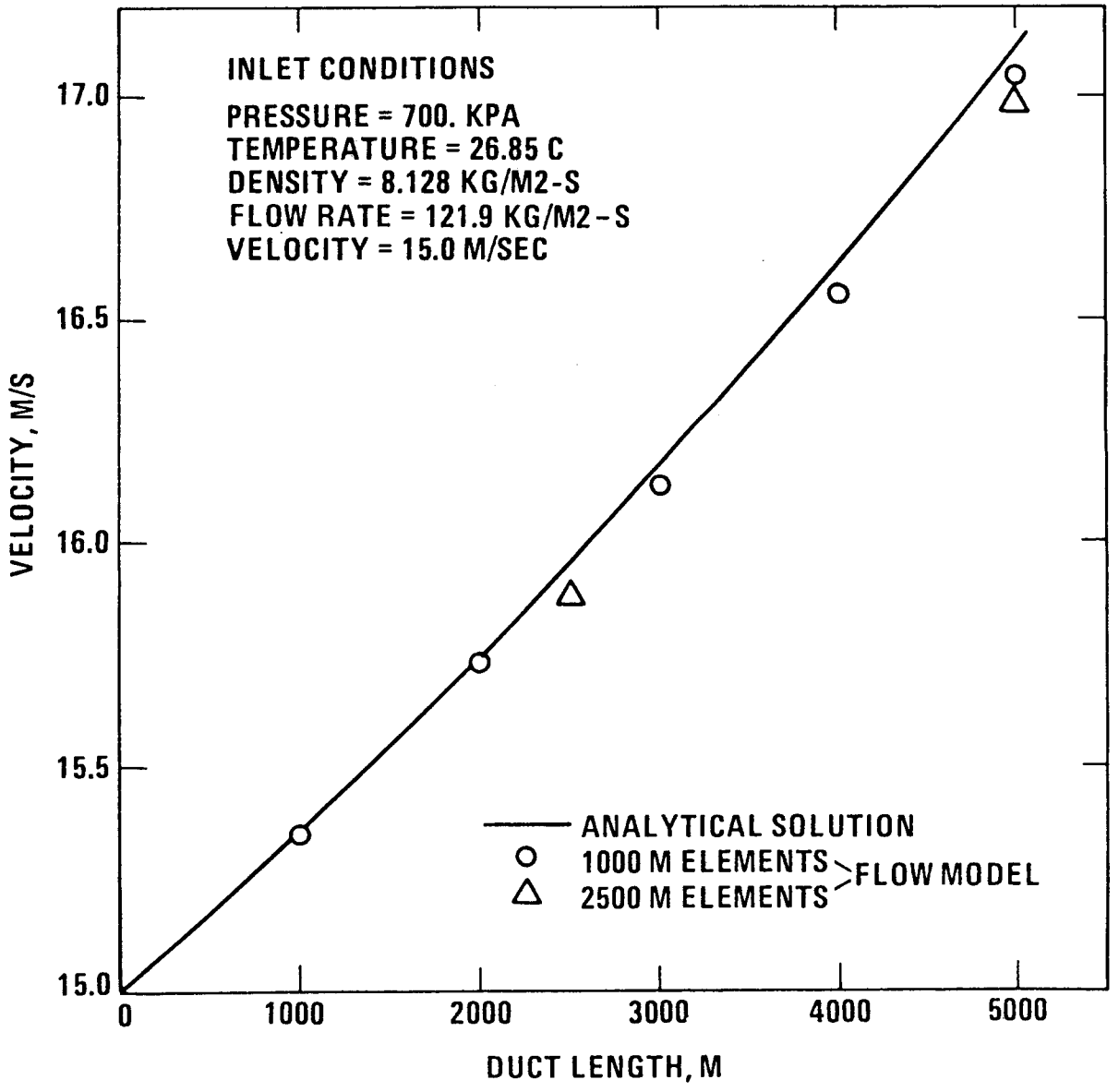

Figure 3. Flow Pressure: Adiabatic Flow with Friction

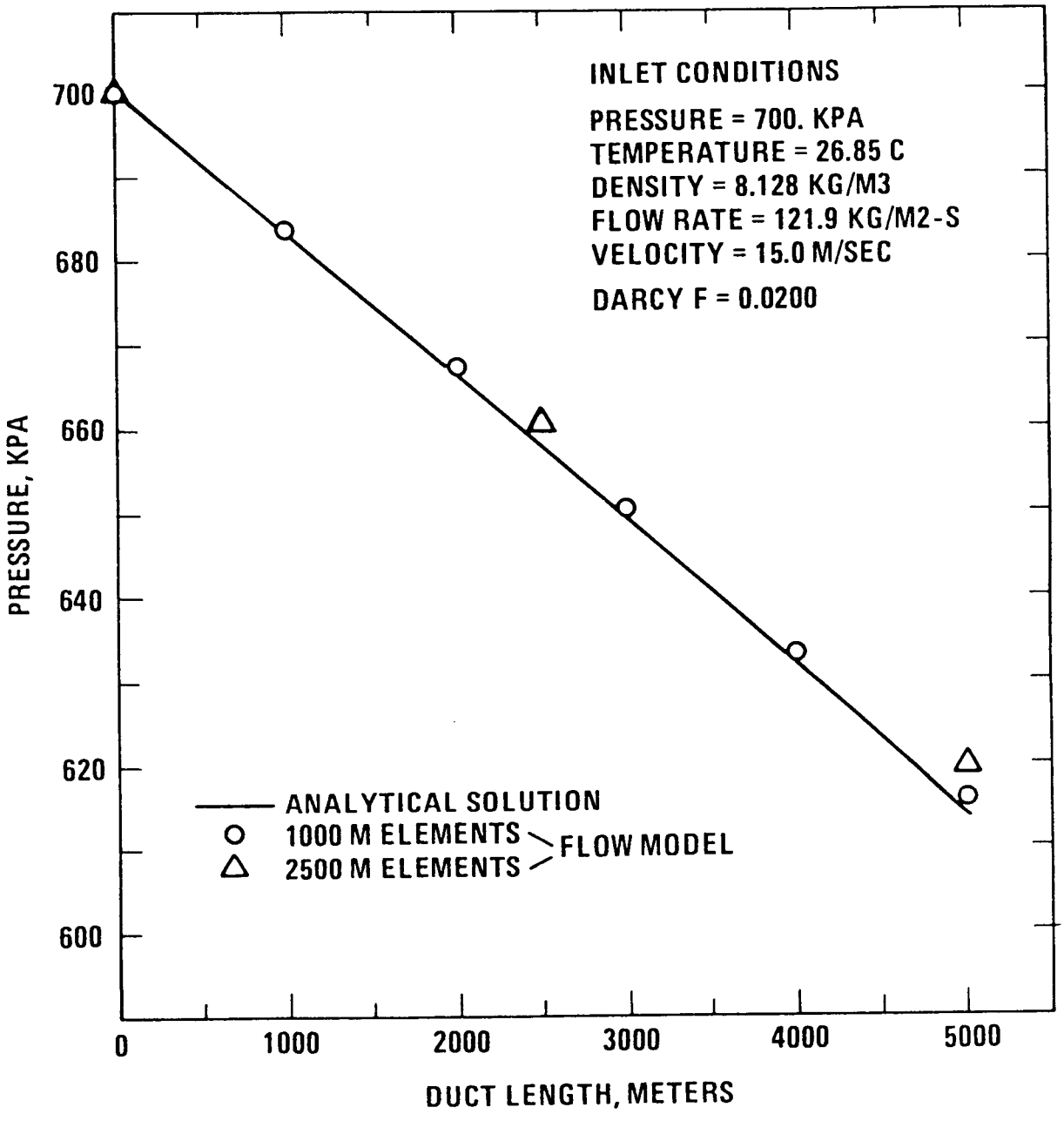

Figure 4. Flow Temperature: Adiabatic Flow with Friction

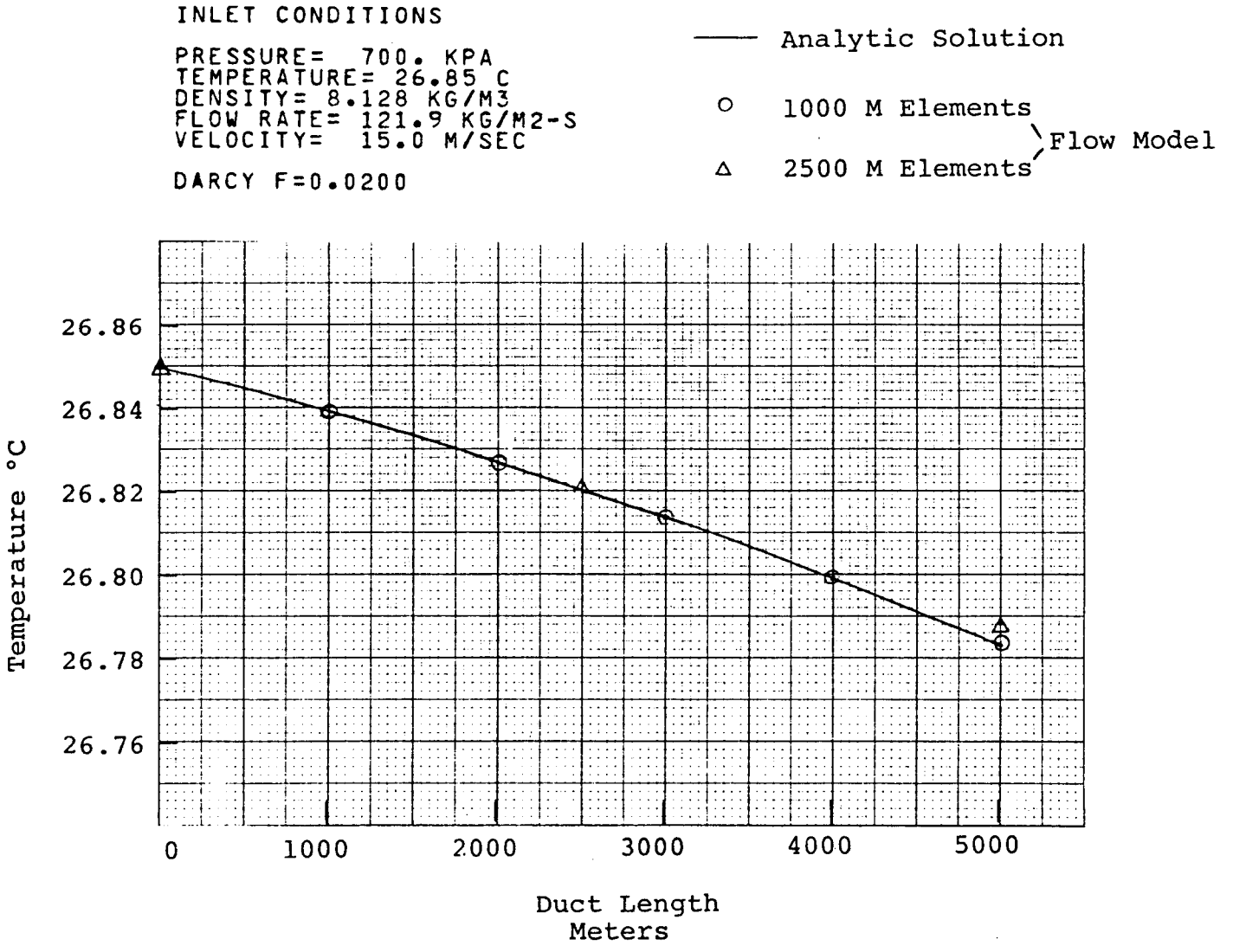

Figure 5. Flow Velocities: Frictionless Flow with Heat Transfer

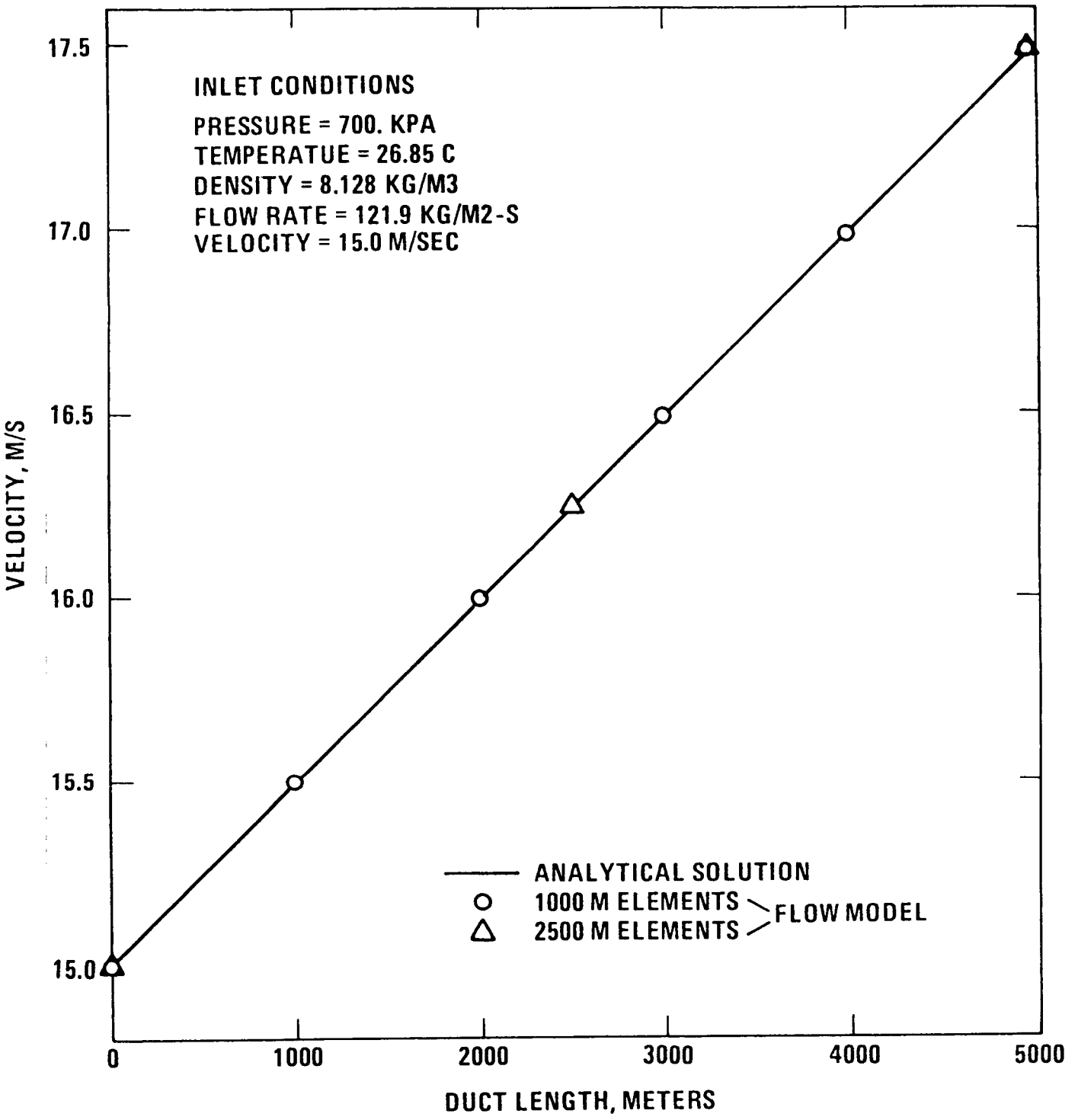

Figure 6. Flow Pressures: Frictionless Flow with Heat Transfer

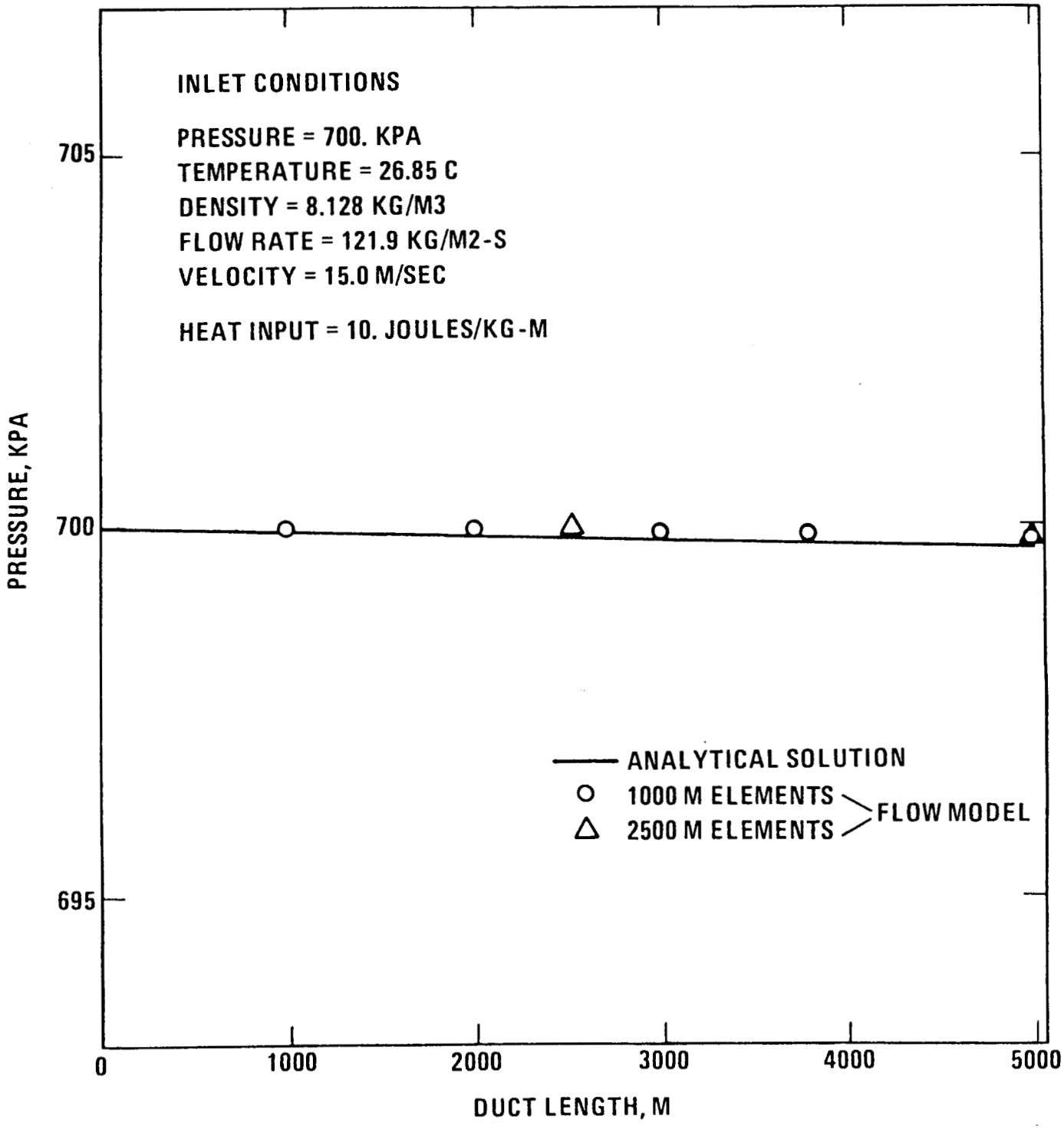

Figure 7. Flow Temperature: Frictionless Flow with Heat Transfer

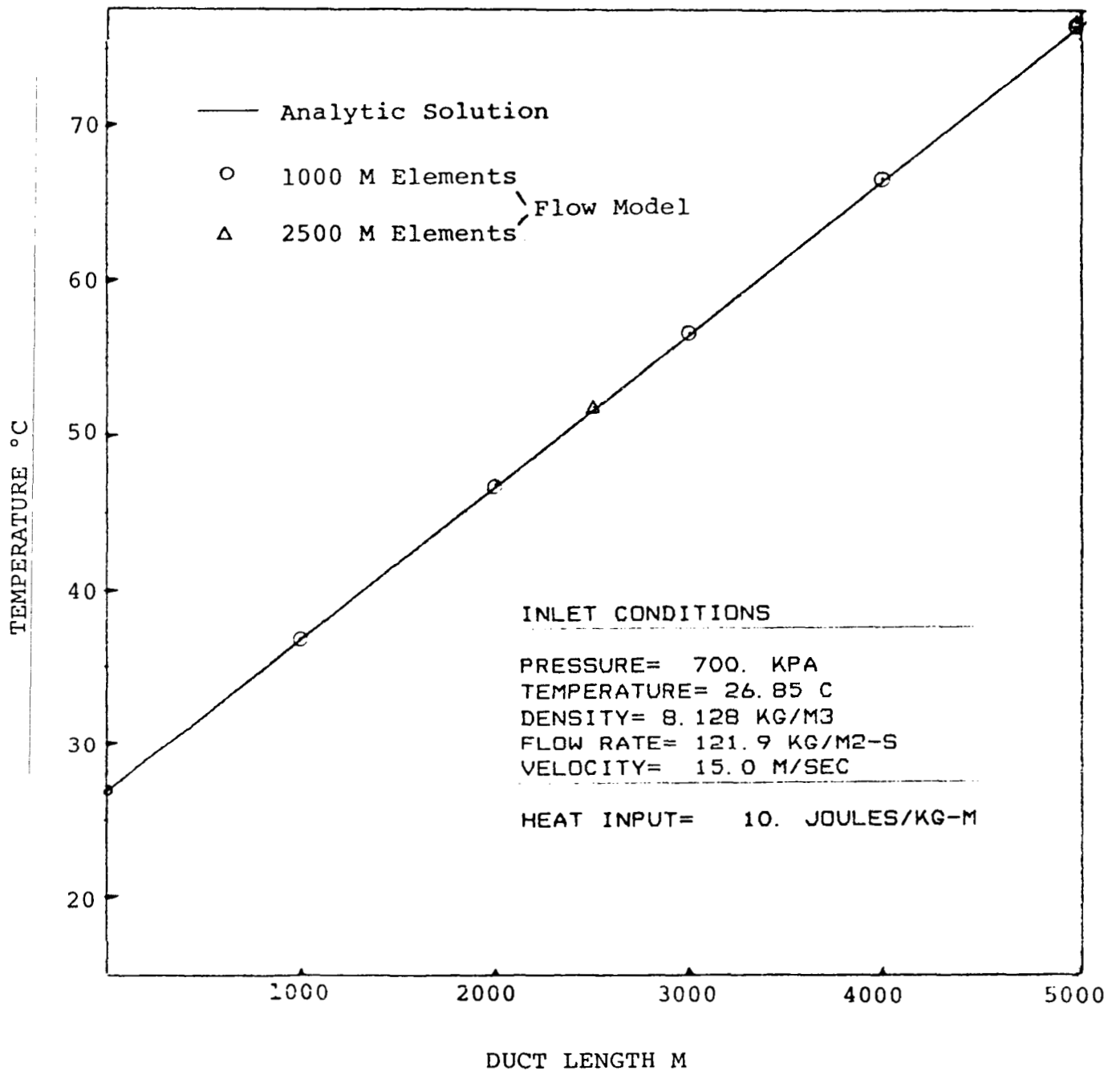

Figure 8. Flow Velocities: Isothermal Flow with Friction

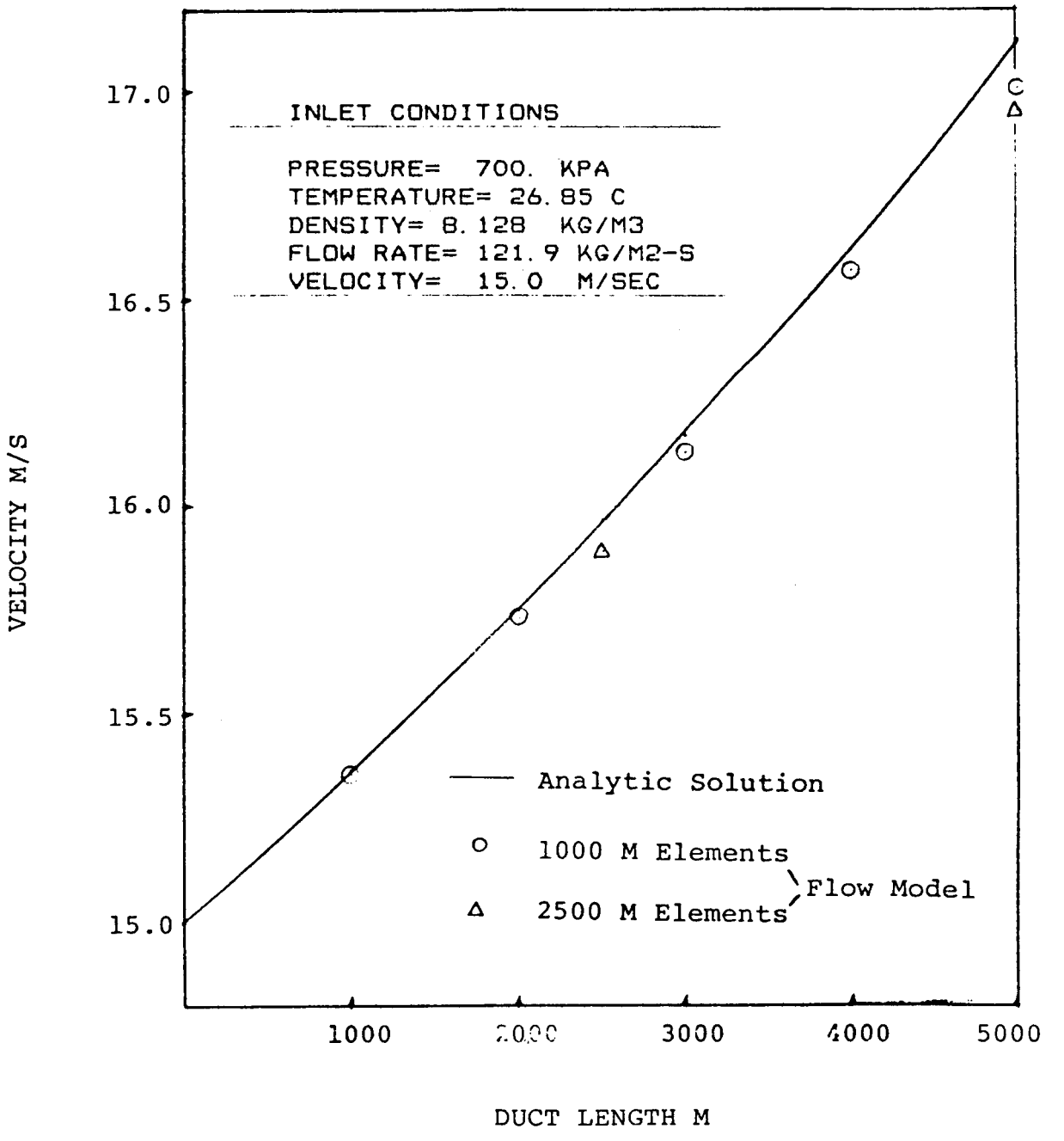

Figure 9. Flow Pressures: Isothermal Flow with Friction

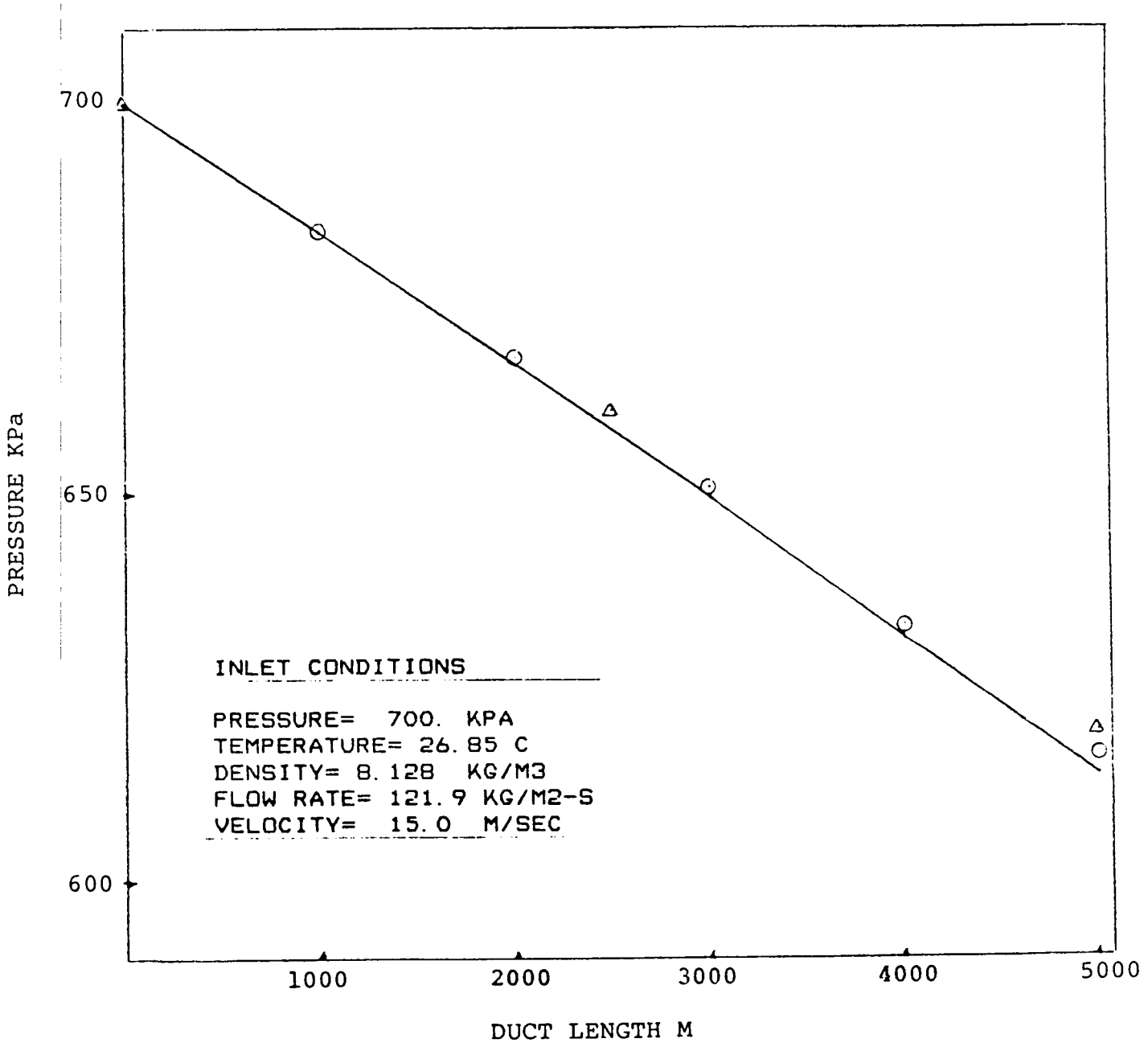

GAS DRILLING

The simulation of the flow of a compressible gas is only part of the analysis necessary to model air and mist drilling. The air or mist drilling problem is really a multi-phase flow situation, where the drill cuttings represent one phase, the air represents a second phase, and water droplets (mist), a third phase.

The addition of the effect of cuttings and mist to the equations already developed requires two changes. First, the effect of the cuttings and mist on momentum equation (3) must be accounted for, and second, the forces exerted on the cuttings and mist must be determined. The principles of multi-phase flow can be applied to both of these effects.

Two basic ideas are sufficient to develop the modified momentum equation. First, the mass flow rate of the cuttings is easy to determine, it's just the product of the penetration rate, the hole area, and the density of the rock. Assuming that the cuttings velocity is known, then a 'density' for the cuttings mass flow rate can be determined:

$$\bar{\rho}_s V_s A = \dot{m}_s = G_s A \qquad (14)$$

This density represents the total mass of cuttings in a volume of the duct divided by the volume of the duct. The ratio of this density to

the actual density of the rock is the volume fraction of the cuttings,

$$\phi = \bar{\rho}_s / \rho_s \tag{15}$$

The density $\bar{\rho}_s$ defined above is called the in-mixture density of the cuttings. The remainder of the volume is assumed to be filled by the air, with an in-mixture density defined:

$$\bar{\rho} = (1-\phi)\rho \tag{16}$$

With these definitions, the cuttings transport equivalents to equations (3),(4), and (5) can be written:

$$\Delta P + G_s \Delta V + G_s \Delta V_s + F + W = 0 \tag{17}$$

$$F = \frac{1}{2} \frac{f}{D} \int_{z_1}^{z_2} (GV + G_s V_s) dZ \tag{18}$$

$$W = \int_{z_1}^{z_2} (\bar{\rho} + \bar{\rho}_s) \cos\alpha \, dZ \tag{19}$$

A more detailed discussion of the ideas used in the development of these equations can be found in references [5], [6], and [7].

The final missing piece is the relationship between the velocity of the air and the velocity of the cuttings. There is a large literature on the data necessary to determine this relationship. For example, in the petroleum engineering literature, there is the work of

Gray [8]. There is also a large literature on terminal settling velocities for solid particles (see reference [5], chapter 1, section 3). The basic equation needed is given by Gray in equation (15) of the appendix to reference [8]. Rewritten in terms of flow variables previously defined, this equation becomes:

$$G_s \Delta V_s + W_s - P = 0 \tag{20}$$

where

$$W_s = \int_{Z_1}^{Z_2} (\rho - \rho_s) \phi g \cos\alpha \, dZ \tag{21}$$

$$P = C_D \frac{1}{\delta} \int_{Z_1}^{Z_2} \rho (V - V_s)^2 dZ \tag{22}$$

The term W_s is the buoyant weight of the cuttings. The term P is the aerodynamic force exerted on the cuttings by the air, with C_D the drag coefficient and δ the ratio of the average particle volume to its cross-sectional area. Values of C_D can be found for various types of rock in references [5] and [8]. The function used to evaluate C_D in GEOTEMP2 is given in appendix A and is valid from Reynolds numbers characteristic of Stokes flow to fully turbulent flow. The term δ was evaluated for an average cutting diameter of 3/8 of an inch. This size is considered to be typical of cuttings at the bit. Higher up the hole, these cuttings get broken into smaller pieces. Because there is no way of predicting the change in average particle size as the cuttings move up the annulus, the average diameter is held fixed at 3/8 of an inch. This assumption

causes the model to overpredict the relative velocity between the air and the cuttings through equation (22). This assumption is conservative because higher air velocities are now needed to lift the cuttings. The assumption used by Angel is that the particle velocity and the air velocity are equal and he notes that this is not conservative.

The same technique is used to solve equations (17) through (22) that was used to solve equations (3) through (5). When an equation similar to equation (7) is defined for the solids, equations (21) and (22) can be integrated, giving:

$$W_s = W_o - \frac{1}{2}(W_o \Delta V_1 / V_{s_1} - \rho_1 g \cos\alpha \, \Delta Z \Delta V / V_1) \tag{23}$$

where

$$W_o = (\rho_{s_1} - \rho_1)\phi g \cos\alpha \, \Delta Z \tag{24}$$

and

$$P = P_o + P_1(\Delta V_s - \Delta V) \tag{25}$$

where

$$P_o = C_D G G_s (V_{s_1} - V_s)^2 \Delta Z / (2\delta \, V_{s_1} V_1) \tag{26}$$

and

$$P_1 = C_D G G_s (V_{s_1}^3 - V_1^3) \Delta Z / (4 \, \delta V_{s_1}^2 V_1^2). \tag{27}$$

Equations (23) and (24) are now substituted into equation (20), so that V_s can be solved for in terms of V. V_s is then eliminated from equation (17), resulting in an equation similar to (9).

The addition of mist to the flowing equations is much simpler than adding the cuttings. The water droplets in a mist are very small, and as a result, the relative velocity between the air and the mist droplets is small. The usual assumption used in two-phase flow analysis is that the air and mist move at the same velocity, and simulations using equation (22) verify this. Equations (17) through (19) are suitable to model mist flow with the following changes: the mass flow and density of the mist replace those for the cuttings and the velocities of the mist and the air are set equal.

The flow equations developed here were incorporated into the GEOTEMP2 wellbore thermal simulator to give a simultaneous solution of the mass, momentum, and energy equations. The technique for solving the energy equation is described in references [2] and [9]. The momentum equations (17) and (20) are solved simultaneously with the energy equation described in reference [9], plus the addition of the kinetic and potential energy terms neglected in the original GEOTEMP formulation. As a test of the code, the following case presented in Angel's paper was calculated for a direct comparison:

5 inch drillpipe

8-3/4 inch hole

90 ft/hr drilling rate

3000 ft/min equivalent gas velocity.

The results of the comparison are presented in Figure 10. The cuttings model predicts higher volume flow rates than Angel's model, which was expected because of the conservative nature of the cuttings model. The cuttings model also shows, however, that the flow rates specified by Angel are adequate to clean the hole, even though they do not satisfy the 3000 ft/min requirement. Figure 11 shows the temperatures predicted by the cuttings model. The temperatures are reasonably near the undisturbed geothermal temperature, which justifies the temperature assumptions used by Angel.

To illustrate the operation of the air drilling model in GEOTEMP2, a sample problem similar to the previous test case is examined in detail in the following discussion. The air drilling simulation is defined by these parameters:

5 inch drill pipe

8-3/4 inch hole

3 3/4 inch bit nozzles

600' 8 inch drill collars

90 ft/hr drilling rate

mist drilling-2 bbl/hr water added

The bottom hole assembly is illustrated in Figure 12. Two cases are

considered here. The first case is air drilling to 9000 ft. The second case duplicates the first case up to the depth of 5400 ft. At this point, mist drilling is started and continued to 9000 ft. This case was run to get a direct comparison between air and mist drilling requirements.

The volume flow rate requirements are shown in Figure 13. The volumes used for the air drilling case are based on the Angel charts, and were adequate to clean the hole. However, in the mist drilling case, significant increases in the volume flow rate were needed when water was added to the air. Figure 14 shows the standpipe pressures needed to maintain the flow rates. A large increase in pressure was needed when mist was used as a drilling fluid. Figure 15 shows the predicted bottom hole velocities for these cases. The predicted cuttings velocities are much lower than the air velocities. Interestingly, the cuttings velocities increase for mist drilling. Because of the higher pressures needed for mist drilling, the bottom hole air density is higher. As a result, the buoyant weight of the cuttings is lower, resulting in a slightly higher velocity.

Figure 10. Volume Flow Rates: Comparison of Angel with Cuttings Model

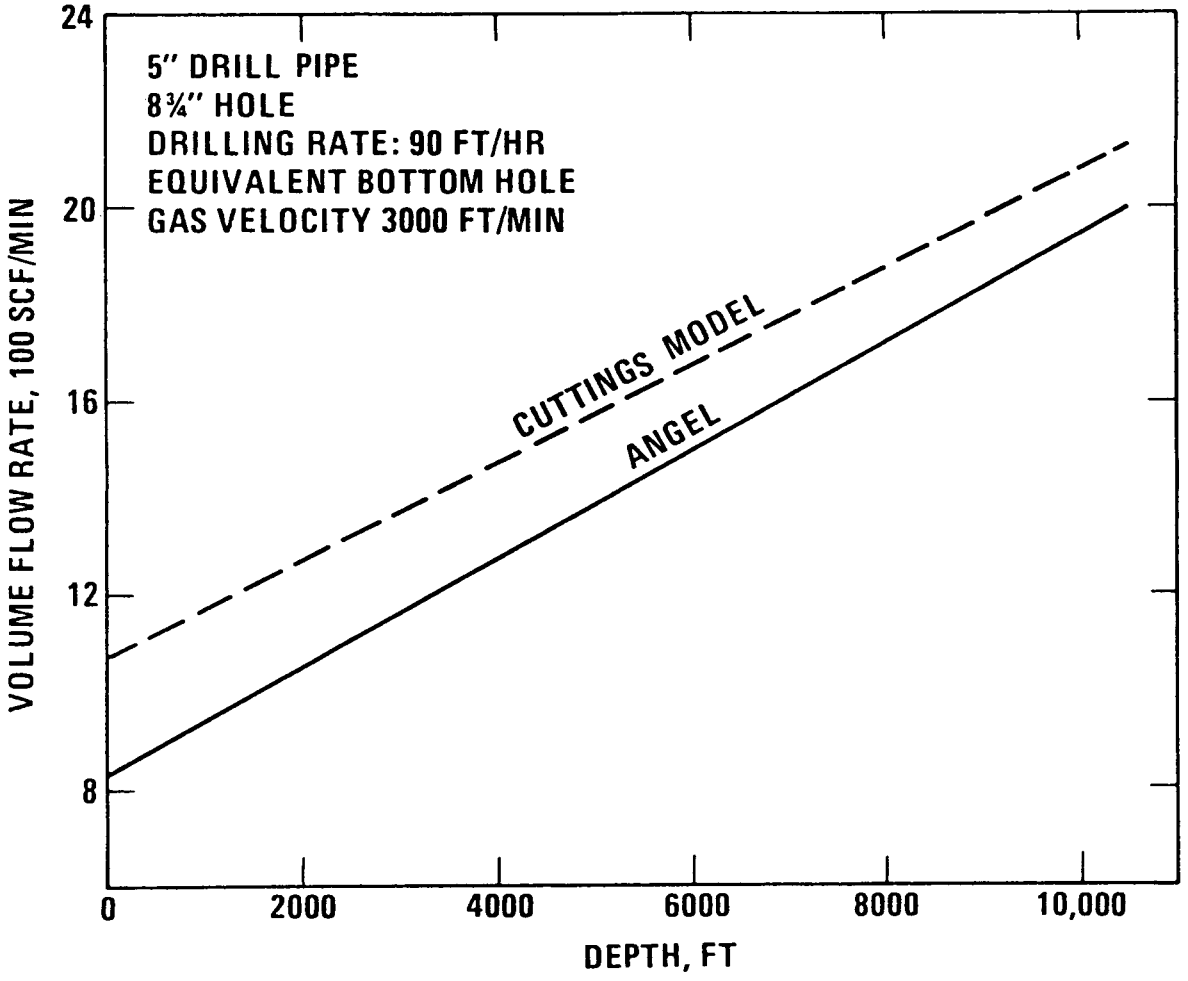

Figure 11. Downhole Temperatures Predicted by Cuttings Model

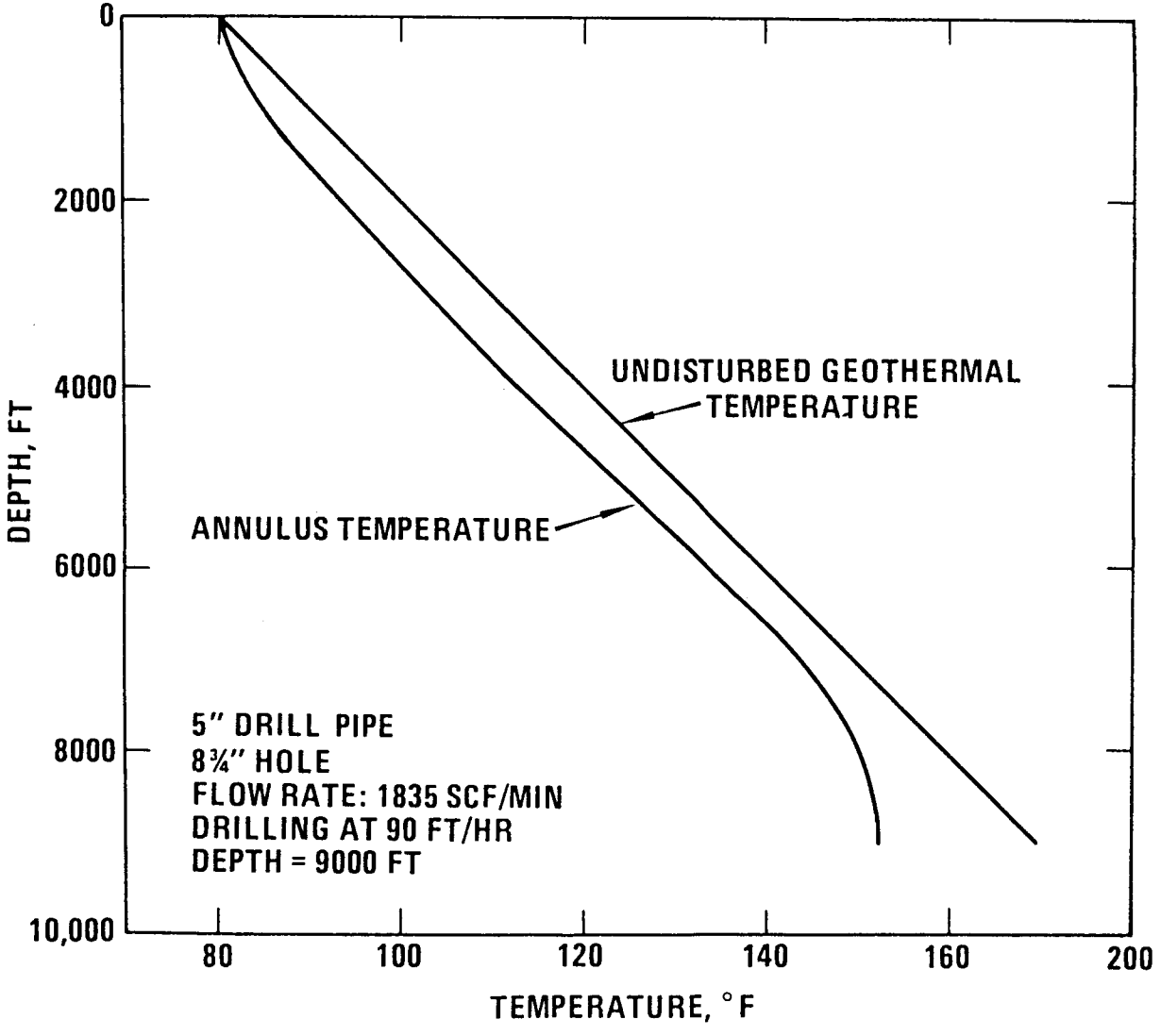

Figure 12. Bottom Hole Assembly: Sample Problem

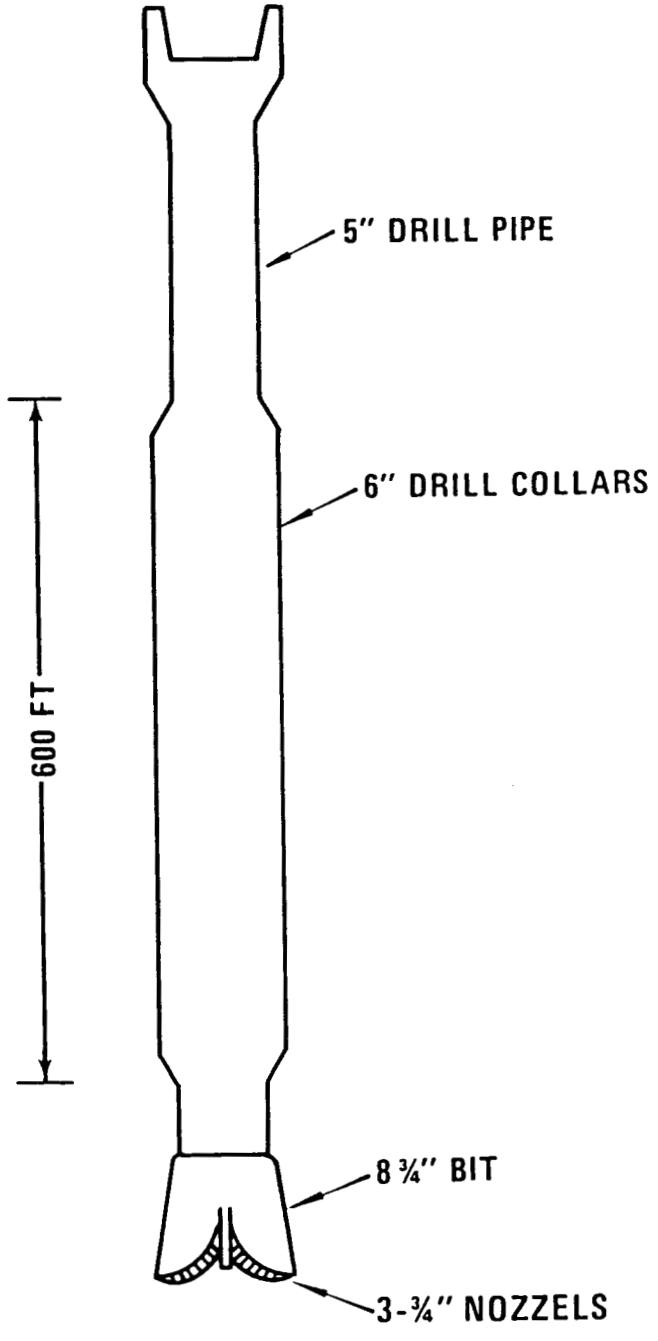

Figure 13. Volume Flow Rates: Air and Mist Drilling

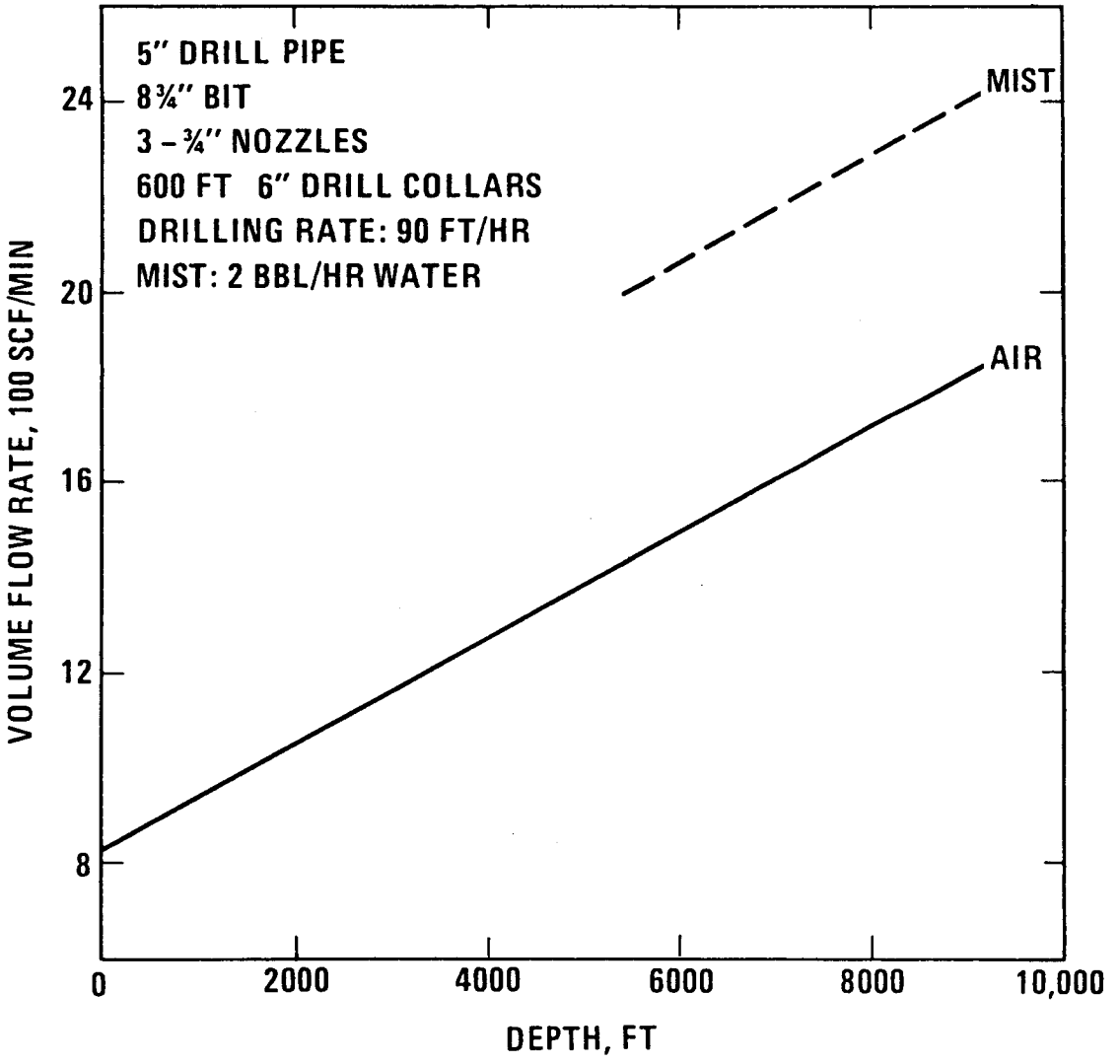

Figure 14. Standpipe Pressures: Air and Mist Drilling

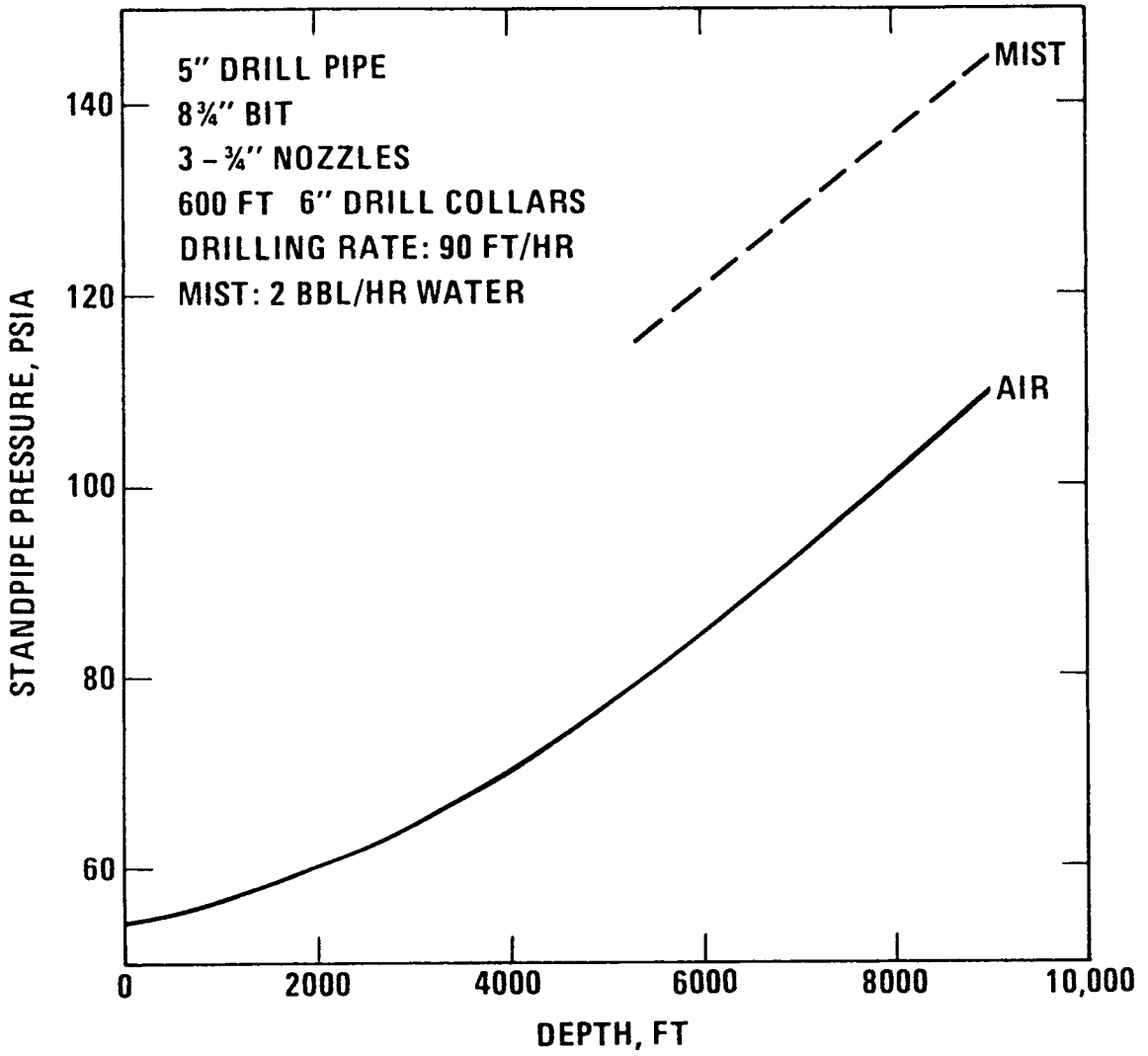

Figure 15. Bottom Hole Velocities: Air and Mist Drilling

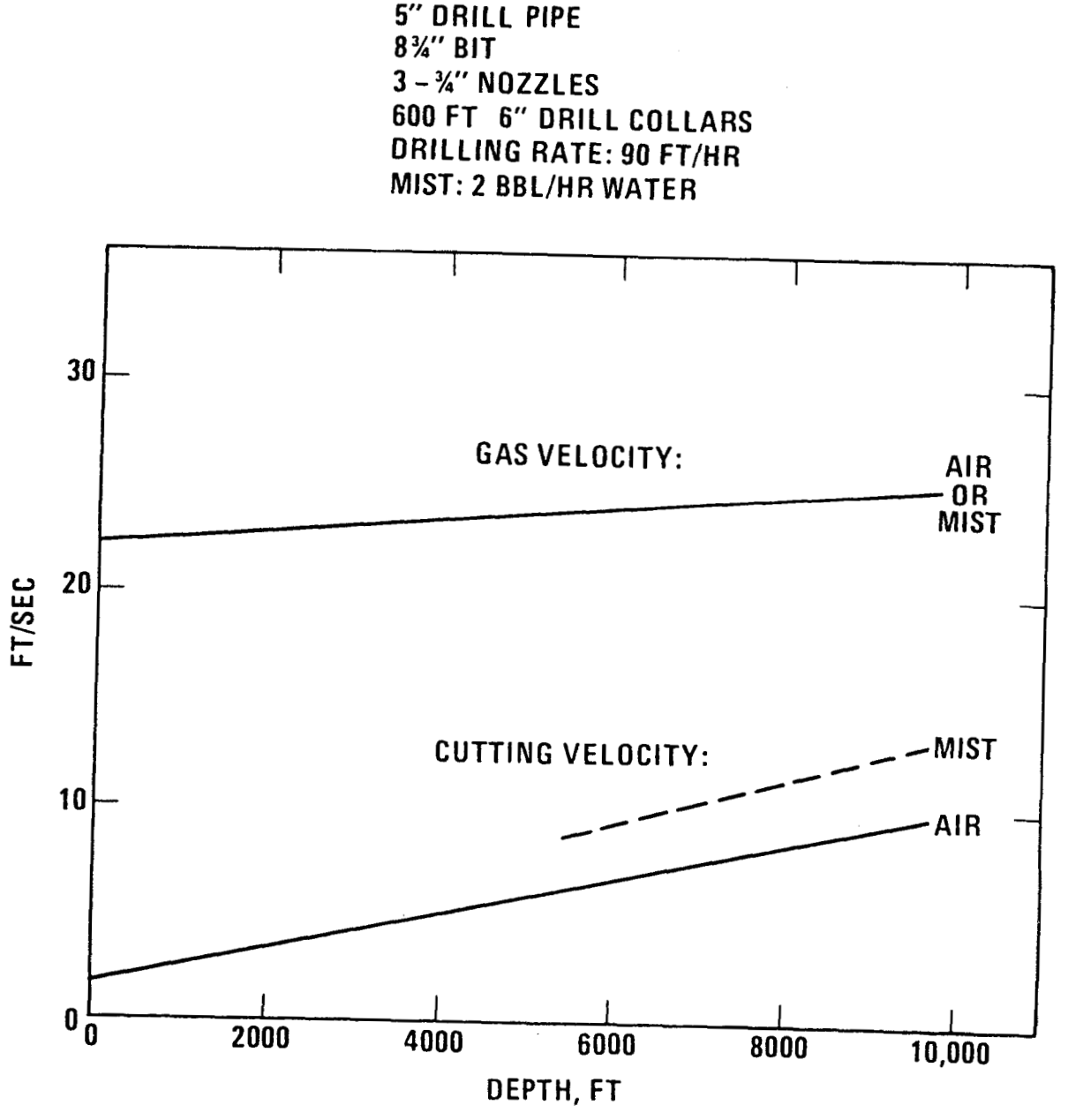

TWO-PHASE FLOW OF STEAM

The full general analysis of the flow of two-phase mixtures does not at present exist. One of the difficulties in achieving such a general analysis is the very different types of flow situations that must be accounted for. For instance, the difference in geometry and velocity of the two phases strongly influence the pressure drop in the tubing. The geometry and velocity of the phases can be very different for the four different flow types or 'regimes'.

Vertical two-phase flow is catagorized by these regimes of flow geometry and velocity. There are four generally accepted catagories of two-phase flow: bubble, slug, transition (frothy), and annular-mist. Figure 16A illustrates a typical bubble flow situation. The pipe is almost completely filled with liquid and the gas phase is small. The gas is distributed as small, randomly sized bubbles which rise at velocities dependent on their size. The gas phase has little effect on the frictional pressure drop caused by the liquid velocity. Figure 16B illustrates slug flow. In this regime, the gas phase takes on more importance. The gas bubbles coalesce and form stable bubbles that span the diameter of the pipe. Slugs of liquid precede and follow these large gas bubbles. The bubble velocity is greater than the liquid velocity. Both the gas and liquid phases have significant effects on the pressure gradient. Figure 16C illustrates 'transition' flow. The

change from continuous liquid phase to continuous gas phase occurs in this regime. Although the liquid effects are important, the gas phase dominates the behavior. Figure 16D illustates annular-mist flow. The gas phase is completely dominant and the liquid phase is carried as droplets.

Bubble flow and annular-mist flow are conceptually fairly simple and can be modeled by methods similar to those used in the gas drilling section of this report. Slug flow is more difficult and transition flow is intractable. The usual method for dealing with slug and transition flow is the use of experiments to develop empirical correlations. Further, experiments are also used to verify the bubble flow and mist flow calculations.

The philosophy in developing a steam injection/steam production model for GEOTEMP2 has been not to work from first principles but rather to find the best available set of correlations and program them as part of the code. One set of two-phase flow correlations in common use in the petroleum industry was developed by Orkiszewski [reference 10]. Orkiszewski tested most of the published two-phase correlations against field data from 148 wells. He was able to select correlations that matched data within 10% for all the flow regimes previously discussed. Espanol, Holmes, and Brown confirmed Orkiszewski's results with independent data [reference 11].

The Orkiszewski correlations are applied in GEOTEMP2 in the

following way. For the inlet conditions to a flow element (Figure 1), the flow regime is identified. The appropriate correlations are then used to determine the frictional and gravitational pressure drop across the element. The exit pressure is determined, and then the saturated temperature is determined from thermodynamic correlations (Appendix C). The energy equation is then solved to determine the phase change in the flow element. For single component calculations, pressure and temperature are independent variables, and the momentum and energy equations are solved simultaneously, as in the previous section.

Determination of Flow Regime

The flow regime limits are defined by four dimensionless numbers:

$(L)_B$ = the bubble flow/slug flow boundary

$(L)_S$ = the slug flow/transition flow boundary

$(L)_M$ = the transition flow/mist flow boundary

$\tilde{v}_g$ = the dimensionless gas velocity

where

$$(L)_B = 1.071 - (0.2218\ V_{ns}^2/D)\ ,\ (L)_B \geq 0.13 \tag{28}$$

$$(L)_S = 50 + 36\tilde{v}_g V_{Sw}/V_{Sg} \tag{29}$$

$$(L)_M = 75 + 84(\tilde{v}_g V_{Sw}/V_{Sg})^{0.75} \tag{30}$$

$$\tilde{v}_g = V_{Sg}(\rho_w/g\sigma)^{.25} \tag{31}$$

$$V_{Sg} = G_g/\rho_g \tag{32}$$

$$V_{Sw} = G_w/\rho_w \quad (33)$$

$$V_{ns} = V_{Sg} + V_{Sw} \quad (34)$$

The notation has been slightly modified from Orkiszewski's original paper to avoid confusion with the previously established notation and to be consistent with the quantities normally used in the pressure drop calculations. For instance, Orkizewski expresses many of his equations in terms of volumetric flow rates. By dividing the volumetric flow rates by the cross-sectional area A, the quantites V_{Sg}, V_{Sw}, and V_{ns} the superficial gas velocity, superficial liquid velocity, and 'no-slip' velocity, are obtained. Another change has been to substitute the subscript w (water) for 1 (liquid) to avoid confusion with the subscript number 1. Note that the densities used in equations (31)-(33) are not the in-mixture densities defined in the gas drilling section, but are the pure component densities. The designation 'superficial' indicates that the velocities defined in equations (32) and (33) are not the actual velocities of the vapor and liquid phases. The no-slip velocity, as it's name indicates, is the velocity that the mixture would move with if there was no relative movement between phases. NOTE: Equation (28) as defined by Orkizewski is not dimensionless unless the coefficient .2218 has units sec^2/ft.

The limits for the various flow regimes are defined in the following way:

Flow Regime	Limits
Bubble	$V_{Sg}/V_{ns} < (L)_B$
Slug	$V_{Sg}/V_{ns} > (L)_B$, $\tilde{v}_g < (L)_S$
Transition	$(L)_M > \tilde{v}_g > (L)_S$
Mist	$\tilde{v}_g > (L)_M$

Pressure Drop Correlations for Two-Phase Flow

The basic equation used to predict pressure drops is the equation for the total change in momentum for the mixture:

$$\Delta P + G_g \Delta V_g + G_w \Delta V_w = F + W \tag{35}$$

where:

$$W = \int_{z_1}^{z_2} \omega g \cos\theta \, dZ \tag{36}$$

and

$$F = \int_{z_1}^{z_2} \tau_f \, dZ \tag{37}$$

The terms ΔV_g and ΔV_w are the changes in the density weighted average velocities of the gas and liquid phases of the mixture. The velocity change terms in equation (35) can be neglected for all flow regimes except mist flow. The terms ω and τ are the mixture density and frictional pressure drop terms respectively. They will be defined by correlations for each flow regime. The integrals in equations (36) and (37) could be evaluated by the same method described in the compressible flow section. In this application, the integrand

is considered constant over the interval ΔZ, which is consistent with Orkizewski's finite difference solution of equation (35).

I. Bubble flow correlations

The void fraction of the gas, ϕ_g, in bubble flow can be expressed:

$$\phi_g = \frac{1}{2}\left[1 + \frac{V_{ns}}{v_b} - \left(\left(1 + \frac{V_{ns}}{v_b}\right)^2 - 4\frac{V_{Sg}}{v_b}\right)^{.5}\right] \tag{38}$$

where v_b is the bubble rise velocity (a recommended value for v_b is .8 ft/sec). The average flowing density ω can now be determined:

$$\omega = (1-\phi_g)\ \rho_w + \phi_g\ \rho_g \tag{39}$$

The frictional gradient term τ_f is:

$$\tau_f = f\rho_w v_w^2/2D \tag{40}$$

where:

$$v_w = V_{Sw}/(1-\phi_g). \tag{41}$$

Although the correlations for bubble flow pressure drop are simple, they are relatively precise. Orkizewski was able to obtain a standard deviation of 5.1% for pure bubble flow situations.

II. Slug Flow Correlations

As previously discussed, slug flow is more complex than bubble flow. It should not come as a surprise that the correlations used to describe slug flow are complicated. The average flowing density ω and the friction pressure drop gradients have the following forms:

$$\omega = \frac{G_g + G_w + \rho_w v_b}{V_{ns} + v_b} + \gamma \rho_w \tag{42}$$

$$\tau_f = \frac{1}{2}\frac{f}{D}\rho_w V_{ns}^2 \left[\frac{V_{Sw} \quad v_b}{V_{ns} + v_b} + \gamma \right] \tag{43}$$

where v_b is the bubble rise velocity and γ is the liquid distribution coefficient. Several correlations are used to describe these variables. First, two special Reynolds numbers are defined that are used in these correlations:

$$N_{Re_s} = \rho_w D V_{ns} / \mu_w = \text{slug Reynolds number} \tag{44}$$

and

$$N_{Re_b} = \rho_w D v_b / \mu_w = \text{bubble Reynolds number} \tag{45}$$

The bubble velocity is now determined from the following relations:

$$v_b = (0.546 + \beta)(gD)^{.5} \quad \text{if } N_{Re_b} < 3000 \tag{46}$$

$$v_b = (0.35 + \beta)(gD)^{.5} \quad \text{if } N_{Re_b} > 8000 \tag{47}$$

and

$$v_b = \frac{1}{2}\alpha + (\alpha^2 + 13.59\mu_w/\rho_w D^{.5})^{.5} \quad \text{for } 3000 < N_{Re_b} < 8000 \tag{48}$$

with

$$\beta = 8.74*10^{-6} N_{Re_s} \tag{49}$$

and

$$\alpha = (0.251 + \beta)(gD)^{.5} \tag{50}$$

Note that equation (48) requires centipoise as the viscosity unit, lb_m/ft^3 as the density unit and feet as the length unit for correct results. For other systems of units modify 13.59 accordingly.

The liquid distribution coefficient γ is determined from the following correlations (see Figure 17):

for $V_{ns} < 10$

$$\gamma = 0.013 \log(\mu_w)/D^{1.38} - 0.681 + 0.232 \log V_{ns} - 0.428 \log D \tag{51}$$

for $V_{ns} > 10$

$$\gamma = 0.045 \log(\mu_w)/D^{0.799} \quad 0.709 - 0.162 \log V_{ns} - 0.888 \log D \tag{52}$$

constrained by

$$\gamma \geq -0.065 V_{ns}$$

and for $V_{ns} > 10$

$$\gamma \geq -\frac{v_b}{V_{ns} + v_b}\left[1 - \frac{\omega}{\rho_w}\right]$$

The friction factor f is evaluated using the correlation given in Appendix A using the slug flow Reynolds number.

III. Transition Flow Correlations

All of the above correlations are based on simplified analytic models. The experimental data are then used to correlate the coefficients in these simplified models. In the case of transition flow, there aren't even any simplified analytic models to work from. The most successful correlations for transition flow have been conceptually the simplest: a linear interpolation between the slug flow correlations and the mist flow correlations. The linear weighting is based on the regime boundary numbers (equations (28)-(30)) and the dimensionless gas velocity (equation (31)). The average flowing density term is computed:

$$\omega = \frac{(L)_M - \tilde{v}_g}{(L)_M - (L)_S}[\omega]_{slug} + \frac{\tilde{v}_g - (L)_S}{(L)_M - (L)_S}[\omega]_{mist} \qquad (53)$$

The friction gradient term is weighted in the same way.

IV. Mist Flow Correlations

The bubble flow correlations treated the two-phase mixture as a slightly modified single component flow. Mist flow represents a similar situation, except the single component is a gas rather than a liquid. Thus, the mist flow correlations have very much the same form as the bubble flow correlations. The average flowing density is given by the same equation as the bubble flow equation (39). In mist flow, however, the gas and liquid phases move at essentially the same velocity, so the equation for the gas volume fraction becomes:

$$\phi_g = V_{Sg}/V_{ns} \tag{54}$$

The friction loss gradient is defined:

$$\tau_f = f\rho_g V_{Sg}/2D \tag{55}$$

and the friction factor is evaluated at the gas Reynolds number

$$N_{Re_g} = \rho_g D V_{Sg}^2/\mu_g \tag{56}$$

Modifications to the relative roughness due to the wetting of the pipe wall are discussed in Appendix A.

Phase Change and the Energy Equation

The flow of two-phase steam is assumed to be at thermodynamic equilibrium in this analysis. To assume a non-equilibrium situation would not be consistent with the philosophy of this development because it would go beyond conventional practice. Further, novel developments of that type would require experimental verification that is not currently available.

The consequence of assuming thermodynamic equilibrium in a two-phase saturated mixture is that the pressure and temperature are not independent. The solution of the momentum equation provides the exit pressure of a flow element. The exit temperature is thus defined through the saturated pressure-temperature relationship (Appendix C). For the energy equation not to be overconstrained, there must be an

additional degree of freedom, and that is change of phase.

The energy equation for a two-phase mixture of steam and water has the following form:

$$\Delta[(h_w + V_w^2/2)G_w + (h_g + V_g^2/2)G_g] + g\cos\theta G_t \Delta Z \underset{\Delta Z}{-\int} Q/A dZ = 0 \qquad (57)$$

where h is the specific enthalpy, Q is the heat flux per unit length of pipe, and the prefix Δ denotes the change in properties from inlet to exit of a flow element. Equation (57) can be expanded and solved for the phase change to obtain the following:

$$\Delta G = (\Delta U_T + \Delta U_q + \Delta U_g)/\Delta u_p \qquad (58)$$

where

$$G_{g_2} = G_{g_1} - \Delta G \qquad (59)$$

$$G_{w_2} = G_{w_1} + \Delta G \qquad (60)$$

$$\Delta U_T = G_{g_1}\Delta(h_g + V_g^2/2) + G_{w_1}\Delta(h_w + V_w^2/2) \qquad (61)$$

$$\Delta U_q = \underset{\Delta Z}{-\int} Q/A \, dZ \qquad (62)$$

$$\Delta U_g = G_t g\cos\theta\Delta Z \qquad (63)$$

and

$$\Delta u_p = h_{g_2} - h_{w_2} + (V_{g_2}^2 - V_{w_2}^2)/2 \qquad (64)$$

Equations (61)-(64) are determined by the inlet and outlet temperatures already determined. Thus, the phase change is computed directly from

equation (58). The exit mass flux densities are then determined from equations (59) and (60).

Two-Phase Heat Transfer

The selection of two-phase heat transfer correlations involved satisfying several objectives. First, the correlation should be consistent with the single phase correlations already in GEOTEMP2. Second, the correlations should make sense theoretically. Further, the correlations should extrapolate smoothly to avoid unreasonable results when used near the limits of applicability.

DeGance and Atherton (reference [12]) recommend the analysis done by Duckler (reference [13]) for developing two-phase correlations. Duckler used dimensional analysis to determine the most reasonable way to develope these correlations. The simplest and most general method Duckler calls 'Case I' similarity.

In 'Case I' similarity, the Reynolds and Prandtl numbers are determined by using density weighted averages. These two-phase dimensionless numbers are determined in the following way.

$$N_{Re_{tp}} = \rho_{tp} V_{ns} D/\mu_{tp} \tag{65}$$

$$N_{Pr_{tp}} = \mu_{tp} C_{tp}/K_{tp} \tag{66}$$

where:

$$\rho_{tp} = \lambda\rho_w + (1-\lambda)\rho_g \tag{67}$$

$$\mu_{tp} = \lambda\mu_w + (1-\lambda)\mu_g \tag{68}$$

$$C_{tp} = \lambda C_w + (1-\lambda)C_g \tag{69}$$

$$K_{tp} = \lambda K_w + (1-\lambda)K_g \tag{70}$$

with

$$\lambda = V_{Sw}/V_{ns} \tag{71}$$

The term C is defined as the specific heat at constant pressure and the term K is the thermal conductivity, subscipts denoting the material. The two-phase Nusselt number is determined as a function of the two-phase Reynolds and Prandtl numbers using the same correlation used by GEOTEMP2 for single phase flows:

$$N_{Nu_{tp}} = 0.023\ N_{Re_{tp}}^{0.80}\ N_{Pr_{tp}}^{0.35} \tag{72}$$

The quantity Q in equation (62) can now be evaluated :

$$Q = \pi K_{tp} N_{Nu_{tp}} \Delta T \tag{73}$$

where ΔT denotes the temperature difference between the two-phase fluid and the pipe wall.

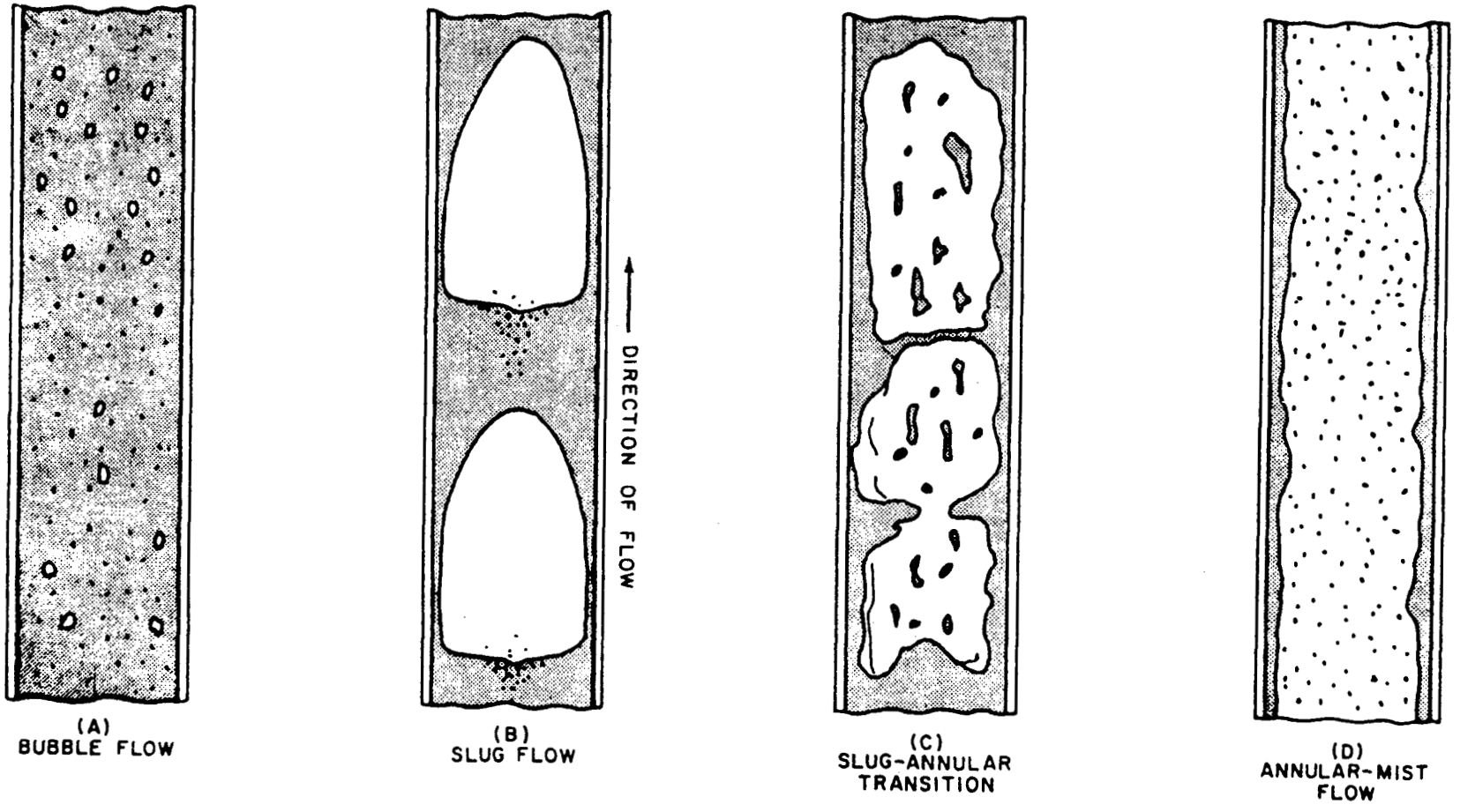

Figure 16. Vertical Two-Phase Flow Regimes

(after Orkiszewski, reference [10])

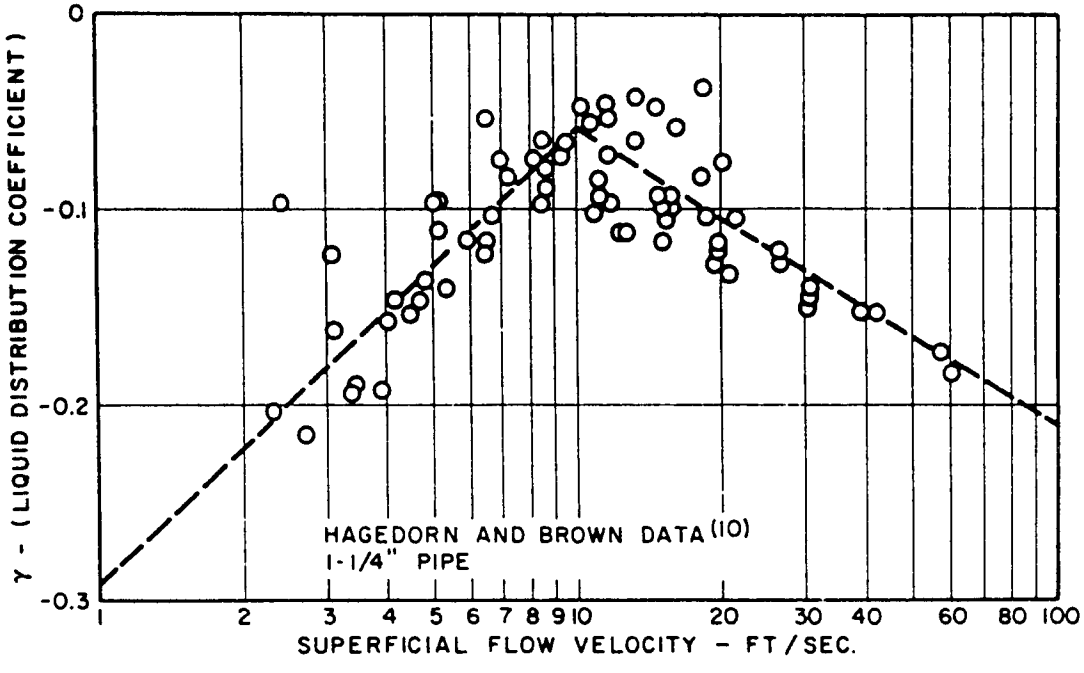

Figure 17. Effect of Velocity on Water Distribution Coefficient

(after Orkiszewski, reference [10])

REFERENCES

1. Angel, R.R.:'Volume Requirements for Air and Gas Drilling', T.P. 4679 Transactions, Vol.210, SPE of AIME, (1957), 325-330.

2. Wooley, Gary R.:'Computing Downhole Temperatures in Circulation, Injection and Production Wells', J.Pet.Tech., (Sept.1980), 1509-1522.

3. Mitchell, R.F.:'Downhole Temperature Prediction for Drilling Geothermal Wells',Proc. Intl. Conf. on Geothermal Drilling and Completion Technology, (Jan.1981), 14.1-14.18

4. Zucrow, Maurice J. and Hoffman, Joe D.,Gas Dynamics, John Wiley and Sons, Inc., New York, (1976).

5. Govier, G.W. and Azziz, K.:The Flow of Complex Mixtures in Pipes, Robert E. Krieger Publishing Co., Huntington, N.Y., (1977).

6. Truedell, C. and Toupin, R.A.:The Classical Field Theories, Handbuch der Physik, Band III/1, Springer, N.Y., (1960).

7. Bowen,R.M., and Wiese, J.C.: 'Diffusion in Mixtures of Elastic Materials', Int.J.Engng Sci., Vol.7, (1969), 689-722.

8. Gray, Kenneth E.,'The Cutting Carrying Capacity of Air at Pressures above Atmospheric', AIME Tech. Paper 874-G, Presented Dallas, (Oct.1957).

9. Wooley, Gary R., Wellbore and Soil Thermal Simulation for Geothermal Wells - Development of Computer Model and Acquisition of Field Temperature Data, submitted to Sandia Laboratories under contract 13-0212, (December 1978).

10. Orkiszewski, J., 'Predicting Two-phase Pressure Drops in Vertical Pipe', J.Pet.Tech.,(June 1967), 829-838.

11. Espanol, J.H., C.S.Holmes, and K.E.Brown, 'Comparison of Existing Multiphase Flow Methods for the Calculation of Pressure Drop in Vertical Wells', Soc.Pet.Engrs., paper no. SPE 2553, (1969).

12. DeGance, Anthony E. and Robert W. Atherton, 'Chemical Engineering Aspects of Two-Phase Flow, Part 3, Transfering Heat in Two-Phase Systems', Chemical Engineering, (May 4,1970), 113-120

13. Duckler, A.E., et.al., 'Frictional Pressure Drop Two-Phase Flow, B. An Approach Through Similarity Analysis', AIChE J.,10, (1964), 44-51.

14. Keenan, J.H. ,F.G.Keyes, et.al.,Steam Tables, John Wiley and Sons,Inc., New York, N.Y., (1969).

APPENDIX A

FRICTION FACTOR AND DRAG COEFFICIENT

FRICTION FACTOR

The friction factor equation used in the development of standard friction factor charts was developed by Colebrook (see Figure 18). This equation accounts for the differences in surface finish of pipes through a factor called the relative roughness. Unfortunately, Colebrook's equation must be solved numerically for the friction factor. The D'Arcy friction factor is evaluated in GEOTEMP2 through an analytic expression developed by Wood (reference [5], page 166). Wood's equation deviates by as much as 4% from Colebrook's equation, but uncertainties in predicting relative roughness are at least this large, so the the two equations should be considered equivalent. The friction factor f is given by:

$$f = 4(a + b\, N_{Re}^{-c}) \qquad \text{(A-1)}$$

where

$$a = .026\ \xi^{.225} + 0.133\ \xi \qquad \text{(A-2)}$$

$$b = 22.\ \xi^{0.44} \qquad \text{(A-3)}$$

$$c = 1.62\ \xi^{0.134} \qquad \text{(A-4)}$$

and

$\xi = k/D$ = relative roughness (A-5)

The following values for k were used in GEOTEMP2:

k (Meters)	Material
.00305	open hole
.000152	galvanized iron
.0000457	steel pipe

In two-phase mist flow, the relative roughness is modified in the following way to account for the liquid phase wetting the pipe wall:

$$k/D = 34\ \sigma/(\rho_g v_g^2 D) \quad \text{for } N_w < 0.005 \tag{A-6}$$

$$k/D = 174.8\ \sigma(N_w)^{0.302}/(\rho_g v_g^2 D) \quad \text{for } N_w > 0.005 \tag{A-7}$$

where

$$N_w = 4.52*10^{-7}(v_g \mu_w/\sigma)^2 \rho_g/\rho_w \tag{A-8}$$

and k/D is restricted to $0.500 > k/D > 0.005$. Equation A-8 should be evaluated for density units of lbm/ft3, viscosity units of centipoise, surface tension (σ) units of lbm/sec and velocity units of ft/sec. The laminar flow friction factor is also computed in GEOTEMP2:

$$f_L = 64/N_{Re} \tag{A-9}$$

and the greater value of equations (1) and (9) is used by GEOTEMP2.

DRAG COEFFICIENT

The drag coefficient used to determine cuttings transport was derived from the terminal settling velocity correlation developed by Swanson (reference [5], page 8):

$$C_D = [a(1 + 6.93b\mu_g/\rho_g dV_n)]^2 \qquad \text{(A-10)}$$

where

$$V_n = \left[\frac{4}{3} g d \frac{(\rho_s - \rho_g)}{\rho_g}\right]^{1/2} \qquad \text{(A-11)}$$

Swanson determined the following values of a and b:

a	b	material
1.277	2.80	irregular quartz
1.082	3.11	cubical galena
.942	3.27	spherical glass
1.870	2.56	irregular KCl
1.072	2.18	irregular sphalerite

The coefficients for irregular quartz were used in GEOTEMP2. The quantity d in equations (A-10) and (A-11) is the particle diameter. The value of 3/8 of an inch was used in GEOTEMP2.

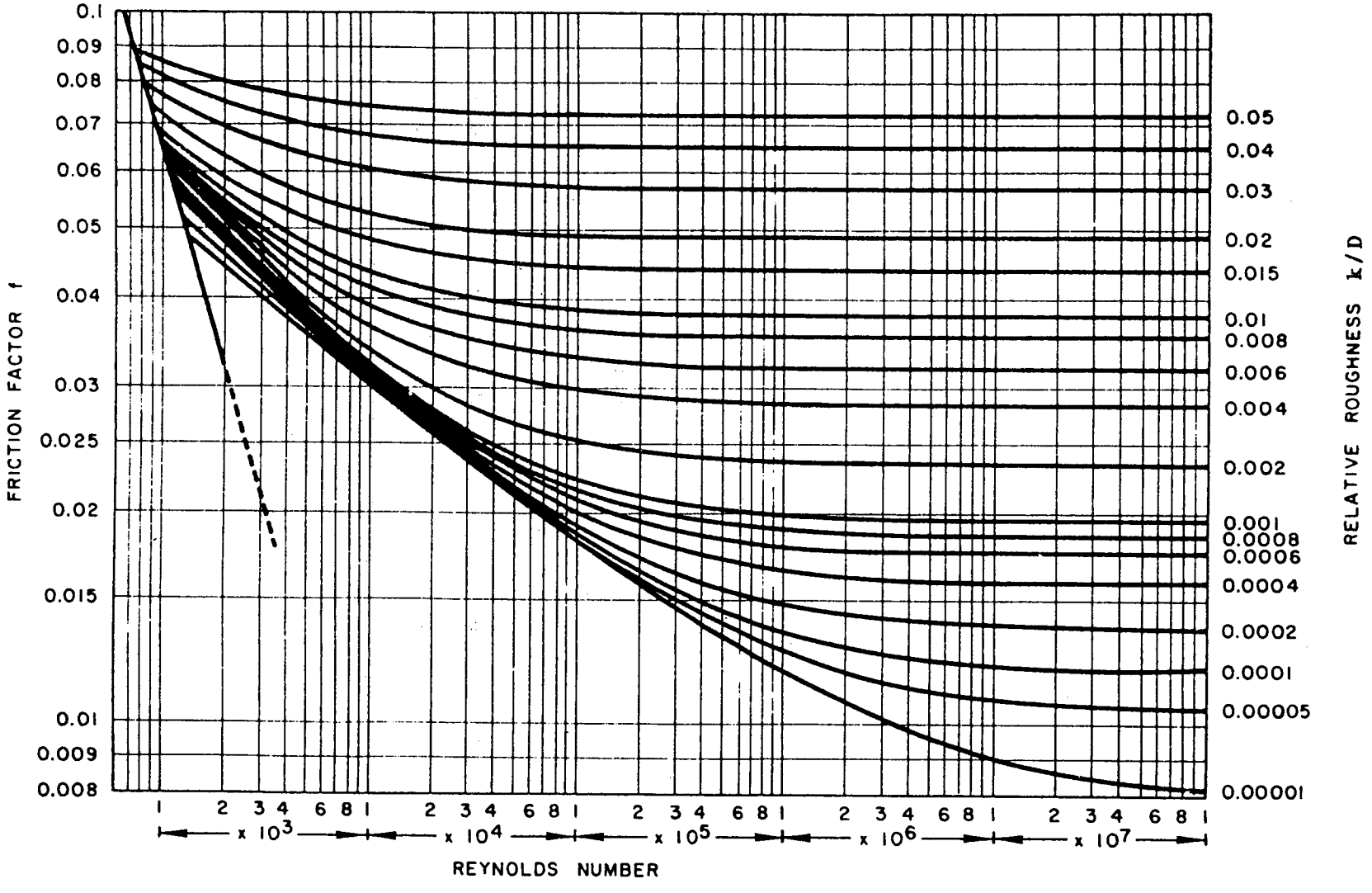

Figure 18. D'Arcy Friction Factor

APPENDIX B

THERMODYNAMIC AND TRANSPORT PROPERTIES OF AIR AND NITROGEN

Air and nitrogen are modeled as ideal gases in GEOTEMP2. For the ranges of pressure and temperature normally expected in gas drilling operations, this is an excellent assumption. Further, the numerical implementation is easy and efficient. The ideal gas thermodynamic equations of state are summarized in the following:

$$P = \rho RT \tag{B-1}$$

and

$$h = C_p T \tag{B-2}$$

where R is called the ideal gas constant and C_p is the specific heat at constant pressure. The following values were used in GEOTEMP2:

Air:

$R = 287.06$ J/kg-K

$C_p = 1004.0$ J/kg-K

Nitrogen:

$R = 296.80$ J/kg-K

$C_p = 1038.3$ J/kg-K

Note that for the units given, density ρ is in kilograms per cubic meter and temperature T is in Kelvins.

The viscosity values used in GEOTEMP2 were determined by the following correlation recommended in reference [4]:

$$\mu = \frac{T^{.5}}{A_0+A_1/T+A_2/T^2+A_3/T^3+A_4/T^4} \qquad \text{(B-3)}$$

with the following values for the coefficients:

	A_0	A_1*10^{-2}	A_2*10^{-4}	A_3*10^{-6}	A_4*10^{-8}
Air	0.552795	2.810892	-13.508340	39.353086	-41.419387
Nitrogen	0.579561	2.847486	-13.232490	37.106107	-37.549675

The thermal conductivity is defined through the following relation:

$$K = C_p \mu / N_{Pr} \qquad \text{(B-4)}$$

where the Prandtl number N_{Pr} is defined for gases through the Eucken equation:

$$N_{Pr} = 4\gamma/(9\gamma - 5). \qquad \text{(B-5)}$$

The term γ in equation (B-5) is the ratio of specific heats of the gas, and in the case of both air and nitrogen, γ equals 1.400 .

APPENDIX C

THERMODYNAMIC AND TRANSPORT PROPERTIES OF STEAM AND WATER

THERMODYNAMIC PROPERTIES

All steam thermodynamic properties used in GEOTEMP2 are derived from the following fundamental equation which expresses the characteristic function α, called the specific Helmholtz free energy, in terms of the independant variables density ρ and temperature T:

$$\alpha = \alpha_0(T) + RT(\ln\rho + \rho Q(\rho,\tau)) \qquad (C\text{-}1)$$

where

$$\alpha_0 = \sum_{i=1}^{6} C_i/\tau^{i-1} + C_7 \ln T + C_8(\ln T)/\tau \qquad (C\text{-}2)$$

$$Q = (\tau-\tau_c)\sum_{j=1}^{7}(\tau-\tau_{aj})^{j-2}B_j \qquad (C\text{-}3)$$

and

$$B_j = \sum_{i=1}^{8} A_{ij}(\rho-\rho_{aj})^{i-1} + \exp(-E\rho)\sum_{i=9}^{10} A_{ij}\rho^{i-9} \qquad (C\text{-}4)$$

In equations (C-1) through (C-4), T denotes temperature in Kelvins, τ denotes 1000/T, ρ denotes density in grams per cubic centimeter, R = .46151 J/g-K, τ = 1.544912, E = 4.8, and

for $j = 1$ $\quad \tau_{aj} = \tau_c \quad \rho_{aj} = 0.634$

for $j > 1$ $\quad = 2.5 \quad = 1.0$

The coefficients for α_0 in joules per gram are as follows:

$C_1 = 1857.065 \quad C_4 = 36.6649 \quad C_7 = 46.$

$C_2 = 3229.12 \quad C_5 = -20.5516 \quad C_8 = -1011.249$

$C_3 = -419.465 \quad C_6 = 4.85233$

and the coefficients Aij are listed in Table I.

The advantage of using a fundamental equation is that all thermodynamic properties can be obtained through derivatives of the characteristic function. Because differentiation, unlike integration, results in no undetermined functions or constants, the information yielded is complete and unambiguous.

The basic thermodynamic relations require:

$$P = \rho^2 \left[\frac{\partial \alpha}{\partial \rho}\right]_\tau \qquad (C\text{-}5)$$

and

$$u = \left[\frac{\partial (\alpha\tau)}{\partial \tau}\right]_\rho \qquad (C\text{-}6)$$

The specific enthalpy can then be derived from the basic definition $h \equiv u + P/\rho$.

TABLE I. COEFFICIENTS Aij

i/j	1	2	3	4
1	29.492937	-5.1985860	6.8335354	-0.1564104
2	-132.13917	7.7779182	-26.149751	-0.72546108
3	274.64632	-33.301902	65.326396	-9.2734289
4	-360.93828	-16.254622	-26.181978	4.3125840
5	342.18431	-177.31074	0.0	0.0
6	-244.50042	127.48742	0.0	0.0
7	155.18535	137.46153	0.0	0.0
8	5.9728487	155.97836	0.0	0.0
9	-410.30848	337.31180	-137.46618	6.7874983
10	-416.05860	-209.88866	-733.96848	10.401717

i/j	5	6	7
1	-6.3972405	-3.9661401	-0.69048554
2	26.409282	15.453061	2.7407416
3	-47.740374	-29.142470	-5.1028070
4	56.323130	29.568796	3.9636085
5	0.0	0.0	0.0
6	0.0	0.0	0.0
7	0.0	0.0	0.0
8	0.0	0.0	0.0
9	136.87317	79.847970	13.041253
10	645.81880	399.17570	71.531353

SATURATED THERMODYNAMIC PROPERTIES

The thermodynamic region where liquid water and vapor coexist is called the two-phase region and the states of the liquid and vapor are called saturated-liquid and saturated-vapor states. Gibb's rule of equilibrium requires that pressure and temperature cannot be independent variables in the two-phase region, thus the saturated pressure Ps is given by the following equation in temperature:

$$P_s = P_c \exp[\tau * 10^{-5} (t_c - t) \sum_{i=1}^{8} F_i (0.65 - 0.01t)^{i-1}] \qquad \text{(C-7)}$$

where Ps is the vapor pressure, t saturation temperature in degrees Celsius, Pc is the critical pressure (220.88 bars), tc critical temperature (374.136 Celsius), τ = 1000/T, and Fi as follows:

$F_1 = -741.9242$ $\quad F_2 = -29.72100$

$F_3 = -11.55286$ $\quad F_4 = -0.8685635$

$F_5 = 0.1094098$ $\quad F_6 = 0.439993$

$F_7 = 0.2520658$ $\quad F_8 = 0.05218684$

Conversely, the saturated temperature as a function of saturated pressure may be needed. The saturated temperature is approximated by:

$$T_s = T_c / [1.73010 - f_s(P)] \qquad \text{(C-8)}$$

where

$$f_s = \sum_{i=1}^{6} B_i (\ln P / \ln P_c)^{i-1} \qquad (C-9)$$

where

$B_1 = -.45800227$ $B_2 = 1.0158658$ $B_3 = .53542626$

$B_4 = .07074624$ $B_5 = -.26191199$ $B_6 = 0.10003160$

The final saturated temperature is converged on through use of equation (C-7). Equation (C-8) is reasonably accurate, so numerical convergence is very fast.

The following two correlations were developed to give saturated vapor and saturated liquid densities. These correlations, combined with equations (C-1),(C-6), and (C-7), will then give all other saturated liquid and vapor thermodynamic properties. Saturated vapor density is given by the following equation:

$$\rho_{satv} = P_s / (TR_{sat}) \qquad (C-10)$$

where

$$R_{sat} = R_2 + R_1 (1 - T_r^x)^{.5}$$

and

$$T_r = (T_s - T_o)/(T_c - T_o)$$

$$x = 2.6 - .6T_r$$

$R_1 = 352.551$ $R_2 = 107.779$

Saturated liquid density is given by the following correlation:

$$\rho_{satl} = \rho_c + (\rho_o - \rho_c)U(T) \qquad \text{(C-11)}$$

where

$$U(T) = (1-T_r^y)^{.5}$$

and

$$y = 1.6160 \exp(.40873\ T_r^5)$$

$$\rho_c = 317.00903 \qquad \rho_o = 1000.0$$

Density units are kilograms per cubic meter and temperature is in Kelvins.

TRANSPORT PROPERTIES

Viscosity for saturated steam is given by the following correlations:

For T < 573.15 Kelvins:

$$\mu_{satv} = [.407t_c + 80.4 - \rho_{satv}(1.8580 - .0059t_c)]*10^{-7} \qquad \text{(C-12)}$$

where $t_c = T - 273.15$

and for T > 573.15 Kelvins:

$$\mu_{satv} = [.407t_c + 80.4 - .088\rho_o + (2.444 - .00117\rho_o)(t_c - 300)]*10^{-7} \quad \text{(C-13)}$$

where $\rho_o = \rho_{satv}(573.15)$ and ρ_c is the critical density.

Viscosity units are Pascal-seconds. Viscosity of saturated water is given in the following correlations:

for T < 573.15

$$\mu_{satl} = [241.4*10^{(247.8/(T-140))}]*10^{-7} \quad \text{(C-14)}$$

and for T > 573.15

$$\mu_{satl} = [\mu_v(\rho_a - \rho_w) + \mu_a(\rho_w - \rho_v)]/(\rho_a - \rho_v) \quad \text{(C-15)}$$

where

$\mu_a = \mu_{satl}(573.15)$ from equation (C-14)

$\mu_v = \mu_{satv}(T)$

$\rho_a = \rho_{satl}(573.15)$

$\rho_w = \rho_{satl}(T)$

and

$\rho_v = \rho_{satv}(T)$

with viscosity units of Pascal-seconds and density units of kilograms per cubic meter.

Thermal conductivity of saturated steam is given by the following correlation:

$$K_{satv} = (K_1 + K_2) * 10^{-3} \qquad \text{(C-16)}$$

where:

$$K_1 = 17.6 + 5.87 * 10^{-2} t + 1.04 * 10^{-4} t^2 - 4.51 * 10^{-8} t^3 \qquad \text{(C-17)}$$

with $t = T - 273.15$, and

$$K_2 = \rho_{satv}(103.51 + 0.4198t - 2.771 * 10^{-5} t^2) * 10^{-3} + 2.1482 * 10^{8} \rho_{satv}^2 / t^{4.2} \qquad \text{(C-18)}$$

The units for K are Watts per meter-Kelvin and the units for ρ are kilograms per cubic meter. The following correlation was used for saturated liquid thermal conductivity:

$$K_{satl} = -.92247 + 2.8395 T_a - 1.800 T_a^2 + .52577 T_a^3 - .07344 T_a^4 \qquad \text{(C-19)}$$

where $T_a = T/273.15$.

The surface tension between water and steam, σ, is given by the following corelation:

$$\sigma = 7.8609 \exp(-77.225/\Delta\mu) \qquad \text{(C-20)}$$

where

$$\Delta\mu = (\mu_{satl} - \mu_{satv}) * 10^{6}$$

Surface tension units are Newtons per square meter, vicosity units are Pascal-seconds.

APPENDIX D

AREA CHANGES IN COMPRESSIBLE FLOW

Because GEOTEMP2 allows discontinuous area changes in the flow tubing (for changes in pipe size), it is necessary to account for the changes in pressure, velocity, and temperature due to this area change. Figure 19 ilustrates the problem to be solved: a compressible gas enters through tubing with area A_1 with pressure P_1, velocity V_1, and temperature T_1, changes area abruptly to area A_2, and exits with pressure P_2, velocity V_2, and temperature T_2. The equations necessary to solve this problem are the conservation of mass, momentum, and energy across the area discontinuity:

$$\dot{m} = \rho_1 A_1 V_1 = \rho_2 A_2 V_2 = G_2 A_2 \qquad \text{(D-1)}$$

$$A_2(P_2 + \rho_2 V_2^2) - A_1(P_1 + \rho_1 V_1^2) = P_b(A_2 - A_1) \qquad \text{(D-2)}$$

and

$$2h_2 + V_2^2 - 2h_1 - V_1^2 = 0 \qquad \text{(D-3)}$$

The term P_b is called the base pressure and for subsonic flow $P_b = P_1$. With this substitution, equation (D-2) reduces to:

$$P_2 - P_1 + G_2(V_2 - V_1) \qquad \text{(D-4)}$$

The final items needed to solve these equations are constitutive equations for the pressure and enthalpy. As an example, the ideal gas equations are a particularly simple set, with

$$P = \rho RT \tag{D-5}$$

and

$$h = C_p T \tag{D-6}$$

where R and C_p are constants. Since the area changes in GEOTEMP2 applications are small, linearized versions of more general equations of state could be used in the same way as equations (D-5) and (D-6). The general case would have to be solved numerically. The exit temperature can be solved for in terms of the exit velocity by using equations (D-3) and (D-6):

$$T_2 = (2h_1 + V_1^2 - V_2^2)/C_p \quad . \tag{D-7}$$

Equation (D-4) is reduced by equation (D-5) to:

$$G_2 RT_2 - P_1 V_1 + G_2 V_2 (V_2 - V_1) = 0 \tag{D-8}$$

With equation (D-7) substituted into (D-8), the resulting equation is a quadratic in terms of V_2. The two roots of the equation represent subsonic and supersonic solutions to the set of equations. The supersonic solution is rejected because it violates the original assumptions about the problem. Imaginary roots imply that the flow chokes going through this area change. Either a

higher inlet pressure or lower flow rate will be required for a real solution.

Figure 19. Tubing Area Changes

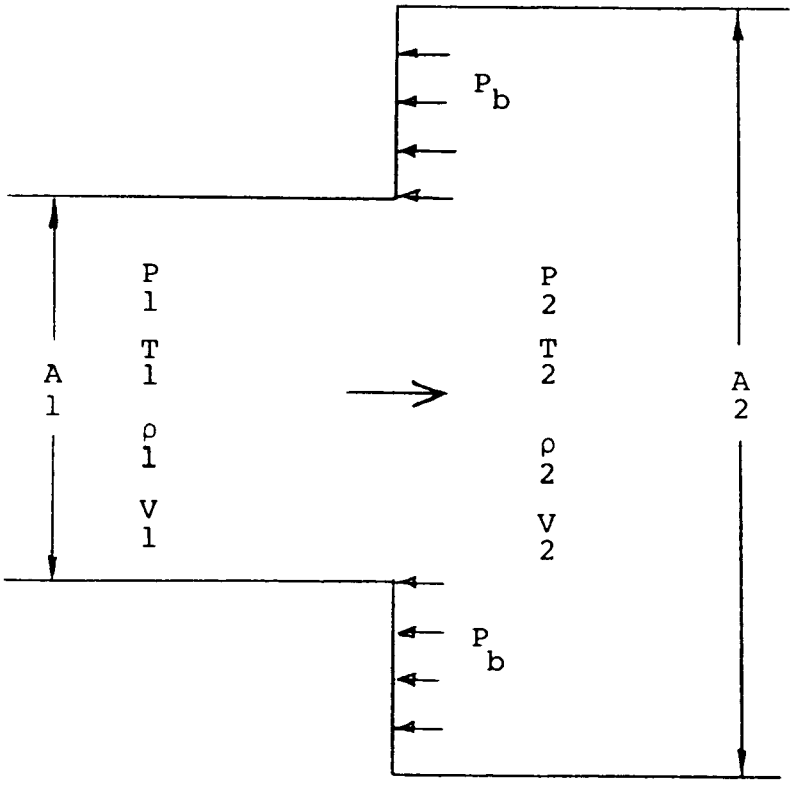

DO NOT MICROFILM

Distribution:
TID-4500-R66-UC-66c (507)

Tom Anderson
Venture Innovations
P.O. Box 35845
Houston, Texas 77035

Ed Bingman
Shell Oil Company
Two Shell Plaza
P.O. Box 2099
Houston, Texas 77001

Larry Diamond
Dyna-Drill
P.O. Box C-19576
Irvine, California 92713

John E. Fontenot
NL Petroleum Services
P.O. Box 60087
Houston, Texas 77205

Dr. Melvin Friedman
Center for Tectonophysics
and Dept. of Geology
Texas A&M University
College Station, Texas 77843

Tom Turner
Phillips Petroleum Company
Geothermal Operations
655 East 4500 South
Salt Lake City, Utah 84107

Jim Kingsolver
Smith Tool
P.O. Box C-19511
Irvine, California 92713

James W. Langford
Security Division
Dresser Industries, Inc.
P.O. Box 24647
Dallas, Texas 75224

Harvey E. Mallory
P.O. Box 54696
Tulsa, Oklahoma 74155

Ed Martin
Superior Oil
Eastern Division
P.O. Box 51108 OCS
Lafayette, Louisiana 70505

Gene Polk
NL Baroid
6400 Uptown Blvd. N.E., 365W
Albuquerque, New Mexico 87110

Del Pyle
Union Geothermal Division
Union Oil Company of California
Union Oil Center
Los Angeles, California 90017

John C. Rowley
Los Alamos National Labs
Mail Stop 570
Los Alamos, New Mexico 87545

Bill Rumbaugh
Otis
P.O. Box 34380
Dallas, Texas 75234

Dwight Smith
Halliburton
Drawer 1431
Duncan, Oklahoma 73533

Tom Warren
Amoco Production Company
P.O. Box 591
Tulsa, Oklahoma 74102

E. L. D. Fooks
Ministry of Works & Development
Private Bag, Taupo
Wairakei, New Zealand

Marion Arnold
Core Laboratories, Inc.
Box 47547
Dallas, Texas 75247

Distribution cont.

Gary McClinton, 2600
Conoco, Inc.
Box 2197
Houston, Texas 77001

D. R. Davies
Koninklijke/Shell Exploratie
en Produktie Laboratorium
Postbus 60, 2280 AB
Rijswijk Z-H
The Netherlands

Michael A. Storms
Deep Sea Drilling Project
U. of California
Scripps Institution of
Oceanography
La Jolla, California 92037

Welby Sweet
Marathon Oil
539 South Main Street
Findley, Ohio 45840

Dr. David D. Balckwell
Professor of Geophysics
Institute for the Study
of Earth and Man
Geothermal Laboratory
Southern Methodist University
Dallas, Texas 75275

Rich Haut
Exxon Production Research
P.O. Box 2189
Houston, Texas 77001

Milton Marks
Dow Chemical Company
Bldg. 1707
Midland, Michigan 48640

John Stalder
Conoco, Inc.
Thermal Recovery Lab
Box 1267
Ponca City, Oklahoma 74601

Professor G. Paul Willhite
Dept. of Chemical and
Petroleum Engineering
University of Kansas
Lawrence, Kansas 66045

Sam Saren
Union Oil
Science & Technology Division
P.O. Box 76
Brea, California 92621

Sam Smith
Union Oil
Science & Technology Division
P.O. Box 76
Brea, California 92621

David McStravick
Baker Packers
P.O. Box 3048
Houston, Texas 77001

U.S. Department of Energy (6)
Geothermal Hydropower
Technologies Division
Forrestal Bldg., CE 324
1000 Independence Ave. S.W.
Washington, D.C. 20585
Attn: J. Bresee
D. Clements
R. Toms
D. Allen
G. Ellis

F. L. Goldsberry
U.S. Department of Energy
Geopressure Projects Office
Suite 8620, Federal Bldg.
515 Rusk Street
Houston, Texas 77002

B. J. Livesay
129 Liverpool
Cardiff, California 92007

Distribution cont.

Pat McGuire
Los Alamos National Labs
Mail Stop 985
Los Alamos, New Mexico 87545

Stephen Pye
Geothermal Division
Union Oil Co. of California
P.O. Box 6854
Santa Rosa, California 95406

Richard Koseluk
Drilling Systems Technology
12950 W. Little York
Houston, Texas 77041

Dennis Goldman
Biological & Earch Sciences
EG&G Idaho, Inc.
P.O. Box 1625
Idaho Falls, Idaho 83401

T. P. Dobbie
Kingston, Reynolds, Thom
& Allardice Limited
P.O. Box 5348, Auckland Ofc.
Auckland, New Zealand

Gene Cannon
Dresser Industries, Inc.
10201 Westheimer Blvd.
Houston, Texas 77042

Ken Green
Dresser Industries, Inc.
10201 Westheimer Blvd.
Houston, Texas 77042

Richard Barker
Dresser Industries, Inc.
10201 Westheimer Blvd.
Houston, Texas 77042

Dr. William L. Perry
Dept. of Mathematics
Texas A&M University
College Station, Texas 77843

Mario Zamora
Imco Mud
P.O. Box 22605
Houston, Texas 77027

Robert Beirute
Amoco Research Center
P.O. Box 591
Tulsa, Oklahoma 74102

Charles Martin
Research & Development Dept.
ARCO Oil & Gas Company
P.O. Box 2819
Dallas, Texas 75221

Mark Cranshaw
Research & Development Dept.
ARCO Oil & Gas Company
P.O. Box 2819
Dallas, Texas 75221

John E. Clarke
Hydril Company
P.O. Box 60458
Houston, Texas 77205

Robert Gaye
Hughes Tool Company
Production Research Dept.
P.O. Box 2539
Houston, Texas 77001

Ronald J. Crook
Chemical Research & Development
Halliburton Services
Drawer 1431
Duncan, Oklahoma 73536

Nancy Jensen
Union Oil Company
461 S. Boylston
Room M-222
Los Angeles, California 90017

Distribution cont.

3141 L. J. Erickson (5)
3151 W. L. Garner (3)
5512 L. A. Mondy
8214 M. A. Pound
9000 G. A. Fowler
9700 E. H. Beckner
9740 R. K. Traeger
9741 J. R. Kelsey (25)
9741 C. C. Carson
9743 H. C. Hardee
9746 B. Granoff
9747 P. J. Hommert
9750 V. L. Dugan
9756 D. Engi
9756 C. Hart

☆U.S. GOVERNMENT PRINTING OFFICE: 1982-0-576-021/589